Aus dem Pathologischem Institut der Universität München
Direktor: Prof. Dr. med. Frederick Klauschen

Proteomics uncover EPHA2 in cetuximab resistant colorectal cancer cell lines as a potential novel therapeutic target

Dissertation
zum Erwerb des Doktorgrades der Medizin
an der Medizinischen Fakultät der
Ludwig-Maximilians-Universität zu München

vorgelegt von
Lucien Edward Torlot
aus
München

2023

Mit Genehmigung der Medizinischen Fakultät

der Universität München

Berichterstatter:	Prof. Dr. Andreas Jung
Mitberichterstatter:	PD Dr. Clemens Gießen-Jung PD. Dr. Johann Spatz Prof. Dr. Martin K. Angele
Mitbetreuung durch den promovierten Mitarbeiter:	PD Dr. Jörg Kumbrink
Dekan:	Prof. Dr. med. Thomas Gudermann

Tag der mündlichen Prüfung: 09.03.2023

Ich widme diese Arbeit

Markus Haubs

*21.07.1958 †24.11.2013

TABLE OF CONTENT

ABSTRACT

Colorectal cancer (CRC) affects more than 50 000 people yearly in Germany alone, with one fifth of patients presenting with UICC stage IV, metastatic disease (mCRC). These patients are typically treated with polychemotherapy combined with targeted anti-EGFR, anti-BRAF or anti-VEGF targeted therapies. Patients with left-sided mCRC and *KRAS, NRAS* and *BRAF* wildtype disease are typically treated with double chemotherapy (FOLFOX or FOLFIRI) combined with the anti-EGFR targeted monoclonal antibodies cetuximab (CET) or panitumumab. Despite the intensive therapy regimens, 5-year survival rates in metastatic disease are as low as 16%, owing to primary treatment resistance or the rapid development of acquired (or secondary) treatment resistance. Both primary and secondary resistance to anti-EGFR therapies, such as CET, have been linked to alterations in the *RAS* genes (mainly *KRAS* and *NRAS*), as these cause self-sufficient mitogenic signalling. RAS small GTPase proteins sit at a crossroad of multiple signalling pathways and constitutively active RAS signalling affects many cellular functions besides mitogenic signalling, making it difficult to assess the full biological implications of oncogenic RAS signalling. This study therefore used mass-spectrometric based proteomics to identify kinome reprogramming in mCRC cell lines with *KRAS* associated, acquired CET resistance in order to investigate the molecular implications of RAS oncogenic signalling and uncover potential second-line therapy options to overcome acquired CET resistance.

The cell line-based model of acquired CET resistance used in this study, comprising two CET sensitive parental cell lines and four isogenic CET resistant cell lines, was characterised by significant changes in the kinome associated with resistance, most of which were specific to individual cell lines. Chemical proteomics identified Ephrin type-A receptor 2 (EPHA2) overexpression as a common feature in all CET resistant cell lines. These resistant cells displayed significantly stronger migration than their parental counterparts (p<0,01) and EPHA2 was found to be a molecular driver of cell migration. Migration rates could be significantly reduced by targeting EPHA2 using RNA interference (RNAi) (p<0,001), ligand stimulation (p<0,001), tyrosine kinase inhibitor treatment (p<0,01) and anti-EPHA2 antibody treatment (p<0,001). These results identify EPHA2 as a potential actionable target for second-line targeted therapies in CET resistant mCRC. This study supported by recent findings emphasises the potential role of EPHA2 as a biomarker and target for precision medicine approaches in mCRC.

ZUSAMMENFASSUNG

In Deutschland erkranken jährlich über 50 000 Menschen am kolorektalen Karzinom (KRK), und etwa jede fünfte Erkrankung manifestiert sich im metastasierten Stadium (UICC Stadium IV). Die Behandlung des metastasiertem KRK (mKRK) umfasst typischerweise eine Polychemotherapie in Kombination mit einer zielgerichteten anti-EGFR, anti-BRAF oder anti-VEGF zielgerichteter Behandlung. Patient*innen mit linksseitigem mKRK und *KRAS*, *NRAS* und *BRAF* Wildtyp werden typischerweise mit einer Chemotherapie Doublette (FOLFOX oder FOLFIRI) und einem der monoklonalen anti-EGFR Antikörper Cetuximab (CET) oder Panitumumab behandelt. Trotz intensiver Therapie beträgt das 5-Jahres Überleben im metastasierten Stadium lediglich 16%, geschuldet durch das Vorhandensein von primäre Resistenzmechanismen oder durch die rasche Entwicklung von sekundären Resistenzmechanismen. Sowohl primäre als auch sekundäre Resistenzen gegen anti-EGFR Therapeutika werden durch Alterationen der *RAS*-Gene (hauptsächlich *KRAS* und *NRAS*) stark begünstigt. Onkogenes RAS hält in Krebszellen mitotische Signalwege aufrecht. Diese kleine GTPasen sitzen an einem molekularen Schaltwerk verschiedener Signalwege und ihre konstitutive Aktivierung beeinflusst viele weitere zelluläre Funktionen als nur mitotische Signalwege, sodass die genaue Wirkung von onkogenem RAS in Krebszellen schwer zu beurteilen ist. Daher untersuchte dieses Forschungsprojekt Änderungen des Kinoms in mKRK-Zelllinien mit sekundärer, *KRAS* assoziierter CET-Resistenz, um die molekulare Auswirkung von onkogenem RAS zu beurteilen und um potenzielle alternative Zielstrukturen für zielgerichtete Therapien zu finden.

Das in diesem Projekt benützte Zelllinien-basierte Model sekundärer CET-Resistenz bestand aus zwei CET-sensitiven parentalen- und vier isogenen CET-resistenten Zelllinien. CET-resistente Zellen wiesen eine stark individuelle Alteration des Kinoms auf. Eine Gemeinsamkeit aller resistenten Zelllinien war die Überexpression von Ephrin Typ-A Rezeptor 2 (EPHA2). Resistente Zellen migrierten signifikant stärker als parentale Zellen ($p<0,01$) und EPHA2 konnte als molekularer Treiber zellulärer Migration identifiziert werden, denn die Migrationsrate konnte durch spezifisches Eingreifen in den EPHA2 Signalweg signifikant reduziert werden. Dies konnte durch RNA-Interferenz (RNAi) ($p<0,001$), Ligandenstimulation ($p<0,001$), Tyrosinkinaseinhibition ($p<0,01$) und anti-EPHA2 Antikörperbehandlung ($p<0,001$) erzielt werden. Diese Ergebnisse identifizieren EPHA2 als potentiell spezifisches Ziel für eine zielgerichtete Therapie in CET-resistentem mKRK. Dieses Projekt, gestützt durch aktuelle wissenschaftliche Erkenntnisse, zeigt die Rolle von EPHA2 als Biomarker und potenzielles Ziel für eine zielgerichtete Behandlungsstrategie in Patient*innen mit mKRK auf.

Disclaimer

This study was conducted between October 2017 and January 2020. This document was finalised in October 2020 and, to the best of the author's knowledge, references the relevant literature published until that date. This study contains experimental data generated by Johanna Albert, M.Sc. It is referenced as so in this thesis and was included in this document for the sake of coherence. The results of this thesis were in the process of submission for publication at the time this thesis was submitted.

ABBREVIATIONS

5-FU	5-fluorouracil	**log_2 FC**	log_2 fold-change
ABC transporters	ATP-binding cassette transporters	**MAPK pathway**	mitogen-activated protein kinase pathway
AMPK-pathway	AMP-activated protein kinase pathway	**mCRC**	metastatic colorectal cancer
APS	ammonium persulfate	**mTOR pathway**	mammalian target of rapamycin pathway
BCR-ABL1	BCR-ABL1 fusion gene	**NGS**	next generation sequencing
BL	baseline tissue biopsy	**NSCLC**	non-small cell lung carcinoma
cDNA	complementary DNA	**ORR**	overall response rate
CET	cetuximab	**OS**	overall survival
CI	confidence interval	**PCA**	principal component analysis
CML	chronic myeloid leukaemia	**PD**	progressive disease tissue biopsy
CMS	consensus molecular subtypes	**pen/strep**	penicillin / streptomycin
CRC	colorectal cancer	**PFS**	progression-free survival
ddH2O	double-distilled water	**pS897**	phosphor-serine 897 (EPHA2)
DiFi-R	cetuximab resistant DiFi cell lines (DiFi-R1 & DiFi-R2)	**pY772**	phospho-tyrosine 772 (EPHA2)
ephrin-A1-Fc	recombinant ephrin-A1 dimerised by fusion to human immunoglobulin G	**Ral pathway**	RAS-Like pathway
FAP	Familial Adenomatous Polyposis	**RAS**	RAS GTPase (includes KRAS, NRAS & HRAS)
FDA	Food & Drug Administration	**RASmt**	RAS mutated (activating mutations)
FDR	false-discovery-rate	**RASwt**	RAS wildtype
Fig.	figure	**REU**	relative expression units
FOLFIRI	combination treatment with folinic acid, 5-fluorouracil, irinotecan	**RNAi**	RNA interference
FOLFOX	combination treatment with folinic acid, 5-fluorouracil, oxaliplatin	**RNAseq**	RNA sequencing
FoxO pathway	forkhead box O pathway	**RT**	room temperature
GAPs	GTPase activating proteins	**RT-PCR**	reverse-transcription polymerase chain reaction
gDNA	genomic DNA	**RT-qPCR**	reverse transcription quantitative real-time polymerase chain reaction
GEO	Gene Expression Omnibus	**SD**	standard deviation
GTP	guanosine triphosphate	**SDS-PAGE**	sodium dodecyl sulphate polyacrylamide gel electrophoresis
GTPase	guanosine triphosphatase	**SEM**	standard error of the mean
HNPCC	Hereditary Nonpolyposis Colorectal Cancer	**siRNA**	short interfering RNA
kDa	kilodalton	**TEMED**	tetramethylethylendiamine
KEGG	Kyoto Encyclopedia of Genes and Genomes	**UICC**	Union Internationale Contre le Cancer
KRASmt	KRAS altered (includes activating mutations and amplification	**α-EPHA2**	anti-EPHA2 antibody
LC/MS-MS	liquid chromatography tandem mass-spectrometry	**α-GFP**	anti-GFP antibody
Lim1215-R	cetuximab resistant Lim1215 cell lines (Lim1215-R1 & Lim1215-R2)		

GENE AND PROTEIN NOMENCLATURE

Protein	Full protein name	Gene	Full gene name
AKT1	RAC-alpha serine/threonine-protein kinase	*AKT1*	AKT serine/threonine kinase 1
BCR-ABL1	BCR-ABL1 fusion protein	*BCR-ABL*	BCR-ABL fusion gene
BRAF	serine/threonine-protein kinase B-raf	*BRAF*	B-Raf proto-oncogene
CCNA2	Cyclin-A2	*CCNA2*	cyclin A2
CCND1	G1/S-specific cyclin-D1	*CCND1*	cyclin D1
CCNH	Cyclin-H	*CCNH*	cyclin H
CDK2	Cyclin-dependent kinase 2	*CDK2*	cyclin dependent kinase 2
CTNNB1	catenin beta-1	*CTNNB1*	catenin beta 1
EGF	Epidermal growth factor	*EGF*	Epidermal growth factor
EGFR	Epidermal growth factor receptor	*EGFR*	Epidermal growth factor receptor
EPHA2	Ephrin type-A receptor 2	*EPHA2*	EPH receptor A2
Ephrin-A1	Ephrin-A1	*EFNA1*	ephrin A1
FAK1	Focal adhesion kinase 1	*PTK2*	protein tyrosine kinase 2
FGF10	Fibroblast growth factor 10	*FGF10*	fibroblast growth factor 10
FGFR1	Fibroblast growth factor receptor 1	*FGFR1*	fibroblast growth factor receptor 1
GFP	Green fluorescent protein	*GFP*	Green fluorescent protein
KRAS	GTPase KRas	*KRAS*	KRAS proto-oncogene
MAPK14	Mitogen-activated protein kinase 14	*MAPK14*	mitogen-activated protein kinase 14
MET	Hepatocyte growth factor receptor	*MET*	MET proto-oncogene
MYC	Myc proto-oncogene protein	*MYC*	MYC proto-oncogene
NF1	Neurofibromin	*NF1*	neurofibromin 1
NRAS	GTPase NRas	*NRAS*	NRAS proto-oncogene
PIK3CA	Phosphatidylinositol 4,5-bisphosphate 3-kinase catalytic subunit alpha isoform	*PIK3CA*	phosphatidylinositol 4,5-bisphosphate 3-kinase catalytic subunit alpha
SRC	Proto-oncogene tyrosine-protein kinase Src	*SRC*	SRC proto-oncogene
TYMS	thymidylate synthetase	*TYMS*	thymidylate synthetase
VEGF-A	Vascular endothelial growth factor A	*VEGFA*	Vascular endothelial growth factor A

FIGURE OVERVIEW

1 Introduction

1.1 Colorectal cancer epidemiology

Colorectal cancer (CRC) ranks as the third cancer-related cause of death in both women and men in Germany and caused approximately 24 000 deaths in Germany in 2018. While hereditary forms of CRC, such as Familial Adenomatous Polyposis (FAP) or Hereditary Nonpolyposis Colorectal Cancer (HNPCC) account for less than 10% of cases, the high incidence of CRC in developed countries can be linked to certain Western life-style factors. These factors mainly include smoking, obesity, lack of physical exercise, alcohol consumption and Western diets of processed or red meat. In Germany, CRC displayed an incidence of 63,6 and 82,9 per 100 000 individuals (women and men respectively) in 2018, with more than half of cases occurring in patients aged 70 and over, and every second case presenting with UICC stage III or IV disease (Fig. 1.1). This is due to the low symptomatic presentation of CRC in early stages. Metastatic disease often presents through the consuming aspect of systemic disease (sometimes referred to as B-symptoms) and through complications secondary to distant metastasis, such as liver failure. In 2018, the 5-year survival rate for metastatic colorectal cancer (mCRC – UICC stage IV) in Germany was16% (Robert Koch-Institut (Hrsg.) und Gesellschaft der epidemiologischen Krebsregister in Deutschland e.V. (Hrsg.), 2021). This has led to increased awareness and the establishment of standardised screening programs in many developed countries, including offering regular colonoscopies for patients aged 50 and over (Leitlinienprogramm Onkologie, 2019).

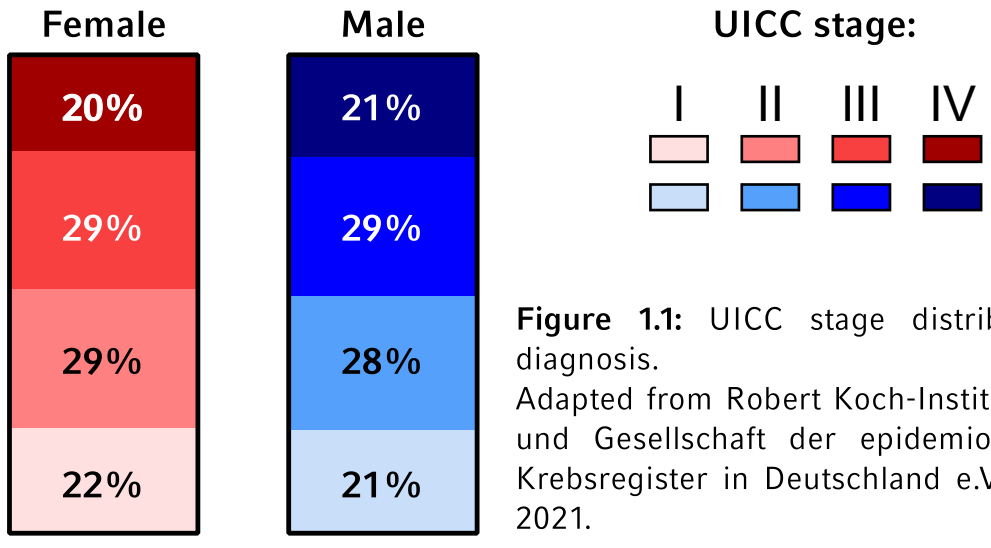

Figure 1.1: UICC stage distribution at diagnosis.
Adapted from Robert Koch-Institut (Hrsg.) und Gesellschaft der epidemiologischen Krebsregister in Deutschland e.V. (Hrsg.), 2021.

1.2 Management of colorectal cancer and targeted therapies

While early-stage CRC can often be cured by surgery alone, mCRC is typically treated through surgery combined with adjuvant (post-surgical) systemic polychemotherapy based on 5-fluorouracil (5-FU) combined with leucovorin (folinic acid) and either

oxaliplatin (FOLFOX) or irinotecan (FOLFIRI) (Leitlinienprogramm Onkologie, 2019). Metastasised rectal carcinoma is sometimes treated with neoadjuvant (pre-surgical) radio-chemotherapy with a goal to debulk the primary tumour before surgical removal. As with other carcinomas, systemic chemotherapy in CRC makes use of cytotoxic drugs that interfere with cell replication in proliferating cells, such as cancer cells, but also cause systemic damage to proliferating, non-cancer tissue (e.g. haematopoietic stem cells) and to drug toxicity specific to the agents used (e.g. neurotoxicity of oxaliplatin). This induces well-known toxic side-effects such as bone marrow depression and puts cancer patients under physiological and psychological strain, limiting the use of such agents (Weinberg, 2014: 806-811).

A more modern approach to treating cancer has been the development of targeted therapies. Targeted therapeutic agents make use of cancer-specific molecular traits, i.e. dysfunctional proteins, which foster the hallmarks of cancer biology: sustained cell proliferation, evasion of growth suppression, replicative immortality, resistance to apoptosis, induction of angiogenesis, induction of migration, invasion and metastasis (Hanahan & Weinberg, 2011). Targeting dysfunctional proteins that drive the hallmarks of cancer has the potential of inducing cytotoxicity in a more cancer-cell selective manner, while reducing side effects caused by systemic cytotoxic effects (Weinberg, 2014: 815-818).
Precision medicine approaches have been adopted into the treatment strategies of patients with mCRC (Leitlinienprogramm Onkologie, 2019). Targeted therapies include the monoclonal anti-epidermal growth factor receptor (EGFR) antibodies cetuximab (CET) and panitumumab, the anti-serine/threonine-protein kinase B-raf (BRAF) directed serine-threonine kinase inhibitor encorafenib as well as the anti-vascular endothelial growth factor A (VEGF-A) antibody bevacizumab. The EGFR is a member of the HER receptor tyrosine kinase family expressed in many epithelial malignant entities (e.g. CRC, non-small cell lung carcinoma, head and neck squamous cell carcinoma) and is involved in sustaining several hallmarks of cancer, including sustained cell proliferation, resistance to apoptosis and induction of angiogenesis (Vincenzi et al., 2010). Anti-EGFR targeted therapies include cetuximab, a chimeric (mouse and human) monoclonal antibody that binds to the extracellular domain of the EGFR, thereby inhibiting binding of its ligand epidermal growth factor (EGF) and other EGF family members. CET inhibits receptor dimerization, autophosphorylation and downstream activation of the mitogen-activated protein kinase (MAPK) pathway amongst others. CET also causes EGFR internalisation and degradation and has also been shown to induce antibody-dependent cellular toxicity (Vincenzi et al., 2010).
Anti-EGFR therapies were shown to display clinical benefit in previously untreated patients with KRAS proto-oncogene (*KRAS*), NRAS proto-oncogene (*NRAS*) and B-Raf proto-oncogene (*BRAF)* wildtype, left-sided mCRC and are widely used in combination with FOLFIRI/FOLFOX or as single-agent treatments (Heinemann et al., 2016; Van Cutsem et al., 2015).

1.3 Primary and secondary treatment resistance

Despite advances in chemotherapy and targeted therapies, which substantially increase progression free survival (PFS) but not overall survival (OS), the mortality rate for CRC patients has plateaued these last decades (Robert Koch-Institut (Hrsg.) und Gesellschaft der epidemiologischen Krebsregister in Deutschland e.V. (Hrsg.), 2021). In most cases, this can be traced back to disease progression under therapy and metastatic dissemination with incurring multi-organ failure. Treatment resistance and associated disease progression have been previously linked to a plethora of factors. Resistance against 5-FU, irinotecan and oxaliplatin have been mainly linked to gene expression changes (thymidylate-synthetase (*TYMS*) overexpression in 5-FU resistance, ATP-binding cassette transporters overexpression in irinotecan resistance and transcriptomic changes in the nucleotide excision DNA-repair pathway in oxaliplatin resistance) (Candeil et al., 2004; De Mattia et al., 2015; Gnoni et al., 2011). In contrast, treatment resistance against anti-EGFR targeted therapies has been linked to genomic alterations (e.g. activating *KRAS*, *NRAS* or *BRAF* gene mutations, but also neurofibromin 1 (*NF1*) mutations in the MAPK-pathway), gene expression changes (e.g. MET proto-oncogene (*MET*) overexpression), changes in DNA-methylation and specific CRC transcriptomic subtypes (consensus molecular subtypes – CMS) (Fig. 1.2) (Lu et al., 2017; Misale et al., 2012, 2014; Song et al., 2014; Stintzing et al., 2019; Van Cutsem et al., 2009; Woolston et al., 2019). Most of the resistance mechanisms described above can occur in both primary and acquired (i.e. secondary) resistance (Fig. 1.2) (Misale et al., 2014). Primary (or *de novo*) resistance refers to stochastically occurring mechanisms of resistance in previously untreated disease. Secondary (or acquired) resistance in contrast is a dynamic process that is believed to result from a Darwinian selection process within the tumour. The selective pressure applied to the tumour through chemotherapy enables stochastic genomic or transcriptomic events which confer resistance and thereby a survival advantage to spread throughout the tumour in a clonal manner (Weinberg, 2014: 806-811). This is accelerated by pre-existing tumour heterogeneity and by adaptive mutability in CRC cells (Molinari et al., 2018; Russo et al., 2019).

1.4 *RAS* genes and cetuximab resistance

As described above, genomic alterations in the *RAS* oncogenes (mainly *KRAS* and *NRAS* in CRC) are biomarkers of resistance against anti-EGFR targeted therapies. RAS proteins are small GTPase proteins, which are active in the GTP-bound configuration. Oncogenic mutations typically target codons 12, 13 and 61 and either inhibit RAS inactivation through GTPase activating proteins (GAPs) or reduce its intrinsic GTPase activity, thereby forcing the oncoprotein in its "ON" state (Weinberg, 2014: 165-169). Constitutively active RAS induces over-activation of the MAPK pathway, thereby rendering upstream signals (e.g. active EGFR signalling) obsolete for mitogenic signalling and lowering the effectiveness of anti-EGFR targeted therapies (Fig. 1.2). Primary *RAS* alterations are central to colorectal carcinogenesis and can be found in up to 30-50% newly diagnosed mCRC patients, predicting poor response to CET (Fearon & Vogelstein, 1990; Karapetis et al., 2008;

Leitlinienprogramm Onkologie, 2019; Van Cutsem et al., 2011). *RAS* alterations have also been observed in acquired CET resistance and occur in 10-45% of patients who have become refractory to CET treatment (Diaz et al., 2012; Misale et al., 2012). Beside the MAPK pathway, oncogenic RAS signalling also activates other signalling pathways (such as the PIK3-AKT-mTOR pathway: phosphoinositide 3-kinase-protein kinase B-mammalian target of rapamycin-pathway) through crosstalk (Weinberg, 2014: 189-192). The downstream molecular signalling patterns induced by oncogenic RAS is therefore complex and it is to this date unclear to what extent crosstalk signalling also confers biological traits implicated in resistance to anti-EGFR therapies and may drive certain aggressive cancer traits. Understanding these complex issues may help identify new treatment strategies to overcome resistance against anti-EGFR targeted therapies, such as CET.

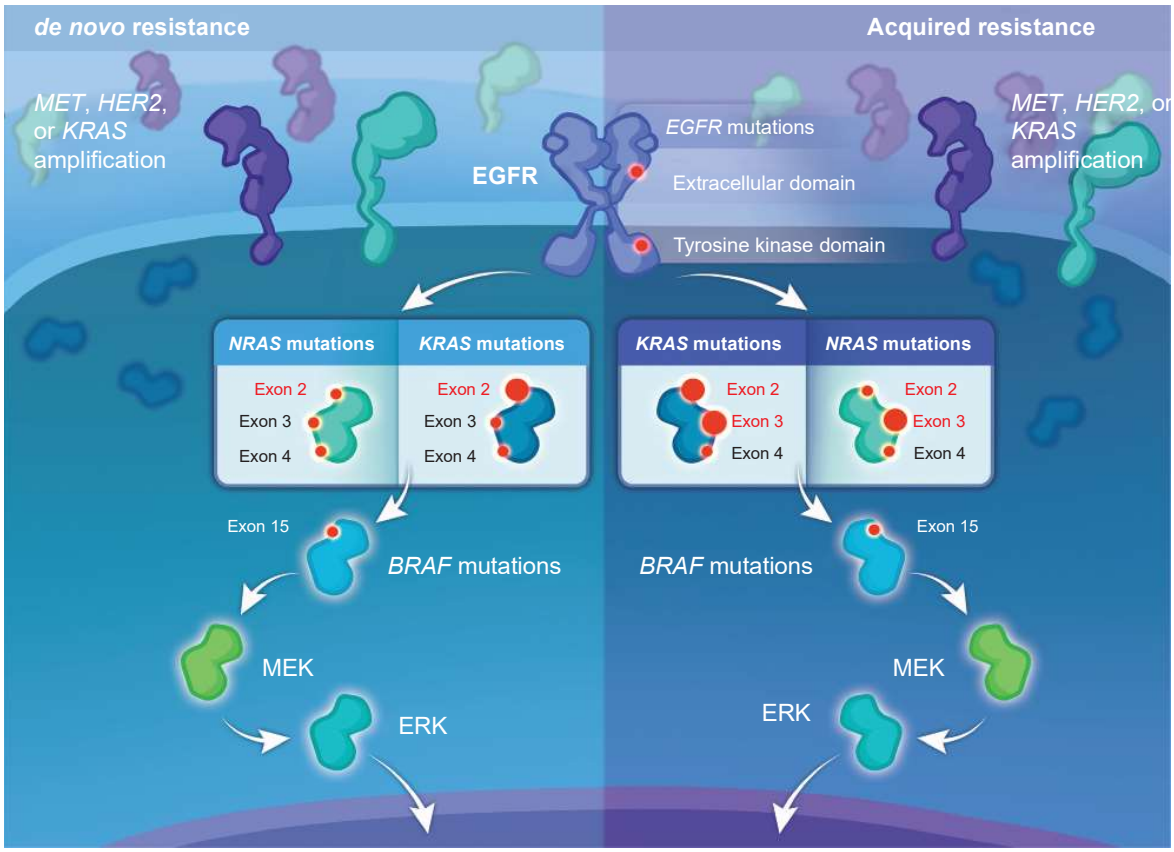

Figure 1.2: CET resistance in mCRC is often linked to genomic alterations, especially in the RAS-RAF-MAPK pathway.
Adapted from Misale et al., 2014.

1.5 Mass-spectrometric based proteomics

Over the decades, researchers in oncology have applied various -omics technologies to elucidate the biology of cancer (Manzoni et al., 2018). The discovery of cellular genes involved in neoplastic growth, starting with the discovery of the SRC oncogene in 1976 triggered a search for further genomic alterations found in cancer (Stehelin et al., 1976). This genomic approach to cancer research yielded a wide list of

oncogenes and tumour suppressor genes frequently mutated in cancer and set the basis for our understanding of cancer biology, including cell proliferation and apoptosis. The establishment of methods for the isolation, stabilisation and analysis of RNA, especially mRNA, enabled the systematic analysis of gene expression levels through identification and quantification of gene specific mRNA levels. This transcriptomic approach to cancer increased the understanding of the dynamics of gene expression, metabolism and cellular signalling. Whole-genome sequencing as well as methylomics, the analysis of DNA methylation patterns, have further deepened the understanding of gene expression regulation and its role in cancer biology. Finally, immunological and mass-spectrometric identification and quantification of proteins and post-transcriptional protein modifications have given insight into molecular cancer phenotypes and the post-translational biology of tumour cells. Proteomics summarise the effect of gene expression, post-translational modifications and protein degradation on cell phenotypes and cell function. The standardised identification and quantification of proteins and protein phosphorylation patterns (phosphoproteomics) can paint a detailed picture of cellular signalling, which is mainly regulated by protein kinases. Protein kinases are proteins involved in cellular signalling that transduce their signals by phosphorylating downstream target proteins. They are a family of 518 proteins, the total of which is referred to as the kinome (Manning et al., 2002). Most signalling pathways, including those involved in mitogenic signalling, metabolism, cellular motility and many others, are regulated by kinases through both kinase activity and kinase expression levels (Blume-Jensen & Hunter, 2001; Fleuren et al., 2016). Many oncogenes encode protein kinases, including SRC proto-oncogene (*SRC*), epidermal growth factor receptor (*EGFR*) and B-Raf proto-oncogene (*BRAF*), and cause kinome reprogramming through over-activation or silencing of kinases and subsequent deregulation of cellular signalling. Protein kinases and the study of kinome reprogramming in cancer have become clinically relevant as recent developments in pharmacology have yielded a wide variety of kinase inhibitors and antibodies targeting specific kinases and signalling pathways deregulated in cancer (Fabbro et al., 2015).

1.6 Aim of this thesis

The complex molecular implications of oncogenic RAS signalling found in acquired CET resistance may through signalling cross-talk confer various biological traits, besides constitutively active mitogenic signalling, leading to anti-EGFR therapy resistance. This research project used a mass-spectrometric based proteomic and phosphoproteomic approach to study kinome reprogramming in the context of *KRAS* altered, acquired CET resistance in mCRC cell lines with the aim of uncovering molecular drivers of CET resistance that may serve as potential second-line therapeutic options.

2 MATERIALS

Table 2.1: Chemicals and solutions

Name	Manufacturer
Acrylamide 30%	Carl Roth GmbH, Karlsruhe, Germany
alamarBlue®	Thermo Fisher Scientific, Waltham, MA, USA
Ammonium persulfate (APS)	Carl Roth GmbH, Karlsruhe, Germany
β-mercaptoethanol	Sigma-Aldrich, St. Louis, MO, USA
Bovine serum albumin 2mg/ml	Bio-Rad Laboratories Inc., Hercules, CA, USA
Cetuximab (Erbitux®)	Merck KGaA, Darmstadt, Germany
cOmplete™ ULTRA protease inhibitor cocktail	Roche Life Science, Penzberg, Germany
Crystal violet solution	Sigma-Aldrich, St. Louis, MO, USA
Dasatinib	MedChemExpress, Monmouth Junction, NJ, USA
Dimethyl Sulfoxide (DMSO)	Sigma-Aldrich, St. Louis, MO, USA
dNTP mix (10mM)	Thermo Fisher Scientific, Waltham, MA, USA
Dulbecco's Modified Eagle's Medium (DMEM)	Biochrom, Berlin, Germany
Ethanol (100%)	Carl Roth GmbH, Karlsruhe, Germany
Foetal bovine serum (FBS)	Biochrom, Berlin, Germany
GeneScan 500LIZ DNA size standard	Applied Biosystems, Foster City, CA, USA
Gylcerol	Carl Roth GmbH, Karlsruhe, Germany
HiDi formamide	Applied Biosystems, Foster City, CA, USA
Horseradish peroxidase (HRP) substrate	Millipore, Burlington, MA, USA
Hydrochloric acid (HCl)	Carl Roth GmbH, Karlsruhe, Germany
Insulin (human recombinant, zinc solution)	Thermo Fisher Scientific, Waltham, MA, USA
Lipofectamin RNAiMAX reagent	Thermo Fisher Scientific, Waltham, MA, USA
Methanol (100%)	Carl Roth GmbH, Karlsruhe, Germany
Milk powder, non-fatty	Carl Roth GmbH, Karlsruhe, Germany
Opti-MEM™ I reduced serum medium	Thermo Fisher Scientific, Waltham, MA, USA
PageRuler™ Plus Prestained Protein Ladder	Thermo Fisher Scientific, Waltham, MA, USA
Phosphate buffered saline (PBS)	Biochrom, Berlin, Germany
Penicillin / streptomycin	Biochrom, Berlin, Germany
PhosSTOP™ phosphatase inhibitor	Roche Life Science, Penzberg, Germany
Random hexamer primers	Thermo Fisher Scientific, Waltham, MA, USA
Probes Master™	Roche Life Science, Penzberg, Germany
Protein Assay Dye	Bio-Rad Laboratories Inc., Hercules, CA, USA
5x Reaction buffer for reverse transcription	Fermentas, Vilnius, Lithuania
RevertAid reverse rranscriptase	Thermo Fisher Scientific, Waltham, MA, USA
Rh/gG1 Fc recombinant human	R&D Systems, Minneapolis, MN, USA
rhEphrin-A1/Fc chimera recombinant human	R&D Systems, Minneapolis, MN, USA
RiboLock RNase Inhibitor	Thermo Fisher Scientific, Waltham, MA, USA
RIPA buffer	Cell Signaling Technology, Danvers, MA, USA

RPMI Media 1640	Biochrom, Berlin, Germany
Running buffer for STR analysis	Applied Biosystems, Foster City, CA, USA
Sodium chloride (NaCl)	Carl Roth GmbH, Karlsruhe, Germany
Sodium dodecyl sulphate (SDS)	Sigma-Aldrich, St. Louis, MO, USA
Sodium hydroxide (NaOH)	Carl Roth GmbH, Karlsruhe, Germany
Tetramethylethylendiamine (TEMED)	Carl Roth GmbH, Karlsruhe, Germany
Trypsin/EDTA solution	Biochrom, Berlin, Germany
Tris base	Carl Roth GmbH, Karlsruhe, Germany
Tween-20	AppliChem GmbH, Darmstadt, Germany
UPL Universal ProbeLibrary	Roche Life Science, Penzberg, Germany

Table 2.2: Consumables

Name	Manufacturer
Cell culture flasks (25cm^2 & 75 cm^2)	Corning, Corning, NY, USA
Eppendorf 1,5ml reaction tubes	Eppendorf, Hamburg, Germany
Falcon® tubes (15ml & 50ml)	Corning, Corning, NY, USA
LightCycler® 480 Multiwell Plate 96	Roche Life Science, Penzberg, Germany
LightCycler® 480 Sealing Foil	Roche Life Science, Penzberg, Germany
Pipette Filter Tips 1000µl, 100µl, 10µl, 2,5µl	Biozym, Hessisch Oldendorf, Germany
Purple Nitrile Xtra gloves	Kimberly-Clark, Irving, TX, USA
Poly-vinylidene difluoride (PVDF) membranes, 0,2µm	Bio-Rad Laboratories Inc., Hercules, CA, USA
Stripettes 2ml, 5ml, 10ml, 25ml	Corning, Corning, NY, USA
Transwell inserts plate 24 well, 8µm pores	Corning, Corning, NY, USA
96-well TC-treated microplates (flat bottomed)	Corning, Corning, NY, USA

Table 2.3: Devices

Name	Manufacturer
ABI3130 genetic analyser	Applied Biosystems, Foster City, CA, USA
Axiovert 25 Inverted Phase Contrast Fluorescent Microscope	Carl Zeiss, Oberkochen, Germany
Centrifuge 5417R	Eppendorf, Hamburg, Germany
Centrifuge Megafuge 40R	Thermo Fisher Scientific, Waltham, MA, USA
Countess cell counting chamber slide	Invitrogen, Carlsbad, CA, USA
Countess II cell counting machine	Invitrogen, Carlsbad, CA, USA
Incubator cell culture HERAcell 240i	Thermo Fisher Scientific, Waltham, MA, USA
Laminar flow hood MAXISAFE 2020	Thermo Fisher Scientific, Waltham, MA, USA
Li-Cor Odyssey FC	Li-Cor, Lincoln, NE, USA
Microscope Primovert	Carl Zeiss, Oberkochen, Germany
Nanodrop 1000 spectrophotometer	Thermo Fisher Scientific, Waltham, MA, USA
PCR cycler Mastercycler® X50	Eppendorf, Hamburg, Germany

Pipetboy 2	INTEGRA Biosciences GmbH, Biebertal, Germany
Pipettes Research plus 1000µl, 100µl, 10µl, 2,5µl	Eppendorf, Hamburg, Germany
qPCR apparatus Mastercycler	Bio-Rad Laboratories Inc., Hercules, CA, USA
Shaker D05-10L	neoLab GmbH, Heidelberg, Germany
Tabletop centrifuge 3-1810	neoLab GmbH, Heidelberg, Germany
Thermomixer comfort	Eppendorf, Hamburg, Germany
Varioskan Flash Photometer	Thermo Fisher Scientific, Waltham, MA, USA
Vortex Genie 2	Scientific Industries, Bohemia, NY, USA
xCell II™ Blot Module	Invitrogen, Carlsbad, CA, USA

Table 2.4: Reaction buffers

Name	Preparation
APS buffer (10%)	5g ammonium persulfate ddH_2O *ad* 50ml
Blocking buffer (5%)	5% (w/) non-fat dry milk powder 100ml 1x TBS-T
Laemmli buffer (4x)	10% SDS 0,5M tris-HCl (pH 6,8) 20% glycerol 10% β-mercaptoethanol ddH_2O *ad* 10ml
Lysis buffer (1x)	1ml 10x RIPA buffer 200µl cOmplete™ ULTRA protease inhibitor solution 200µl 10x PhosSTOP phosphatase inhibitor solution ddH_2O *ad* 10ml
Phosphatase inhibitor solution (10x)	1 PhosSTOP phosphatase inhibitor tablet Dissolved in 2ml ddH_2O
Protease inhibitor solution (10x)	1 cOmplete™ ULTRA protease inhibitor tablet Dissolved in 2ml ddH_2O
Running buffer (10x)	30g tris base 144g glycerol 10g SDS ddH_2O *ad* 1000ml
Running buffer (1x)	100ml 10x running buffer 900ml ddH_2O
TBS buffer (20x)	121g tris base 80g NaCl ddH_2O *ad* 1000ml HCl / NaOH *ad* pH=7,5
TBS-T wash buffer (1x)	50ml 20x TBS buffer 950ml ddH_2O 1ml Tween 20

Transfer buffer (10x)	30g tris base 144g glycerol ddH_2O *ad* 1000ml
Transfer buffer (1x)	100ml 10x transfer buffer 100ml methanol 100% ddH_2O *ad* 1000ml
Tris-HCl (1x, pH 6,8)	1M tris base 100ml ddH_2O HCl / NaOH *ad* pH=6,8
Tris-HCl (1x, pH 8,8)	1,5M tris base 500ml ddH_2O HCl / NaOH *ad* pH=8,8

Table 2.5: Kits

Name	Manufacturer
Multiplex PCR kit	Qiagen, Hilden, Germany
PCR Mycoplasma Test Kit	AppliChem GmbH, Darmstadt, Germany
QIAamp DNA Mini Kit	Qiagen, Hilden, Germany
RNeasy Mini Kit	Qiagen, Hilden, Germany

Table 2.6: Cell lines

Cell line	Organism	CET sensitivity	*KRAS* gene
Lim1215	*Homo sapiens*	sensitive	wildtype
Lim1215-R1	*Homo sapiens*	resistant	c.34G>C mutation
Lim1215-R2	*Homo sapiens*	resistant	c.38G>A mutation
DiFi	*Homo sapiens*	sensitive	wildtype
DiFi-R1	*Homo sapiens*	resistant	amplification
DiFi-R2	*Homo sapiens*	resistant	amplification

Table 2.7: Antibodies

Primary antibody	Host species	Dilution	Manufacturer
α-EPHA2 (clone 1C11A12)	Mouse	1/2000	Invitrogen, Carlsbad, CA, USA
α-EPHA2 (clone AF3035)	Goat	5µg/ml	Biotechne, Minneapolis, MN, USA
α-GFP (clone AF4240)	Goat	5µg/ml	Biotechne, Minneapolis, MN, USA
α-tubulin (clone TU-01)	Mouse	1/15000	Invitrogen, Carlsbad, CA, USA

Secondary antibody	Host species	Dilution	Manufacturer
α-mouse	Rabbit	1/15000	Acris Antibodies GmbH, San Diego, CA, USA

Table 2.8: siRNA

Name	Target sequence	Manufacturer
siEPHA2	CAGCGCCAAGUAAACAGGGUA	Qiagen, Hilden, Germany
siControl	ACAACGAAGCUCCGUCCCUACCGAA	Thermo Fisher Scientific, Waltham, MA, USA

Table 2.9: Primer sequences

Name	UPL #	Working concentration	Sequence	Manufacturer
EPHA2 F	#89	500nM	CCCCAAGTTCGCTGACAT	biomers.net GmbH, Ulm, Germany
EPHA2 R			GGGGAGCCGGATAGACAC	biomers.net GmbH, Ulm, Germany
GAPDH F	#60	300nM	AGCCACATCGCTCAGACAC	biomers.net GmbH, Ulm, Germany
GAPDH R			GCCCAATACGACCAAATCC	biomers.net GmbH, Ulm, Germany

3 METHODS

3.1 CELL LINES AND CELL CULTURE

Cell culture

This project was based on two cell line models of acquired CET resistance established in Dr. Alberto Bardelli's laboratory (Candiolo Cancer Institute, Italy) and kindly provided by him (Misale et al., 2012). In short, CET sensitive CRC cell lines Lim1215 and DiFi were subjected to continuous CET treatment using two different treatment protocols until four isogenic resistant cell lines (Lim1215-R1, Lim1215-R2, DiFi-R1 & DiFi-R2) were established. Lim1215-R (Lim1215-R1 & Lim1215-R2) cell lines independently developed activating KRAS proto-oncogene mutations (*KRAS* codon 2, respectively p.G12R and p.G13D) and DiFi-R (DiFi-R1 & DiFi-R2) cell lines independently developed *KRAS* amplifications as genomic mechanisms of CET resistance (Misale et al., 2012).

The identity of all cell lines was confirmed by Short Tandem Repeat (STR) testing as described below. All cells were routinely tested for *Mycoplasma* contamination using the PCR Mycoplasma Kit (AppliChem, Darmstadt, Germany) following the manufacturer's instructions.

All cell culture experiments were performed in a sterile environment. Cells were kept at 37°C and 5% CO_2. Lim1215 and Lim1215-R cells were cultured in RPMI-1640 medium (Biochrom, Berlin, Germany) supplemented with 5% (v/v) foetal bovine serum (FBS, Biochrom), 1% (v/v) penicillin/streptomycin (pen/strep, Biochrom) and 1µg/ml recombinant insulin (Thermo Fisher Scientific, Waltham, MA, USA). DiFi & DiFi-R cell lines were grown in DMEM/Ham F-12 medium (Biochrom) supplemented with 10% (v/v) FBS and 1% (v/v) pen/strep. In order to maintain CET resistance Lim1215-R and DiFi-R were cultured for 3 days per week in the presence of 25µg/ml CET (Erbitux®, Merck KGaA, Darmstadt, Germany), acquired from the Munich University Hospital pharmacy. Cells were cultured in 25cm^2 or 75cm^2 flasks and passaged three times weekly at a maximum confluence of 80%. Cells were passaged by removing the supernatant medium, washing the cells with PBS (Biochrom) and detaching them using trypsin (Biochrom). Trypsin was neutralised using FBS-containing medium and removed by sedimenting cells and removing supernatants. Cells were then resuspended at approximately 15% of the original density in fresh medium and transferred into new flasks. All experiments were performed in biological replicates using cells at different passages (5 to 25). In order to store them, cells were detached, washed and the cell pellet resuspended in freezing medium containing 90% FBS and 10% DMSO (Sigma-Aldrich, St. Louis, MO, USA) and transferred into cryotubes. Cells were stored at -80°C or in liquid nitrogen. To thaw cells, cryotubes were briefly warmed in a 30°C water bath and the cell-suspension diluted in fresh medium. Cells were sedimented, the supernatant removed, and the cells resuspended in fresh medium and transferred into cell culture flasks.

STR analysis and Next-Generation-Sequencing

Cell identity was confirmed both by STR analysis and by Next-Generation-Sequencing (NGS). Genomic DNA (gDNA) from cell lines was prepared using QIAamp DNA Mini Kit DNA extraction kits according to the manufacturer's instructions (Qiagen, Hilden, Germany). For STR testing, a multiplex PCR amplifying 9 common microsatellite loci (D16S539, D13S317, D5S818, D7S820, CSF1PO, TPOX, TH01, vWA and amelogenin – AMG) within the gDNA was performed using Multiplex PCR kits according to the manufacturer's instructions (Qiagen, Hilden, Germany) (Dirks & Drexler, 2013). Amplified fragments were diluted in HiDi formamide (Applied Biosystems, Foster City, CA, USA) together with GeneScan 500LIZ DNA size standard, denaturated (3 min at 95°C) and loaded onto an ABI 3130 genetic analyser (Applied Biosystems). Fragment lengths were mapped using GeneMapper 4.0 and cross-referenced using the Cellosaurus STR Similarity Search Tool (CLASTR: https://web.expasy.org/cellosaurus-str-search/). Cell line identity scores are calculated using the Tanabe algorithm (Robin et al., 2020). Cell lines were considered authentic when the STR profile displayed a ≥80% match when compared to the reference profile (Reid et al., 2004).

Cell line identity for resistant cell lines was also confirmed using NGS in order to confirm oncogenic point mutations and amplifications. NGS analysis was performed by the Munich University Hospital Department of Molecular Pathology using the OncoMine™ Focus Assay on an IonTorrent™ PGM (personal genome machine) (Thermo Fisher Scientific). Uncovered genomic alterations were cross-referenced with previously published data on the respective cell lines (Misale et al., 2012).

3.2 Proteomics

For the proteomic analysis, parental and resistant cell lines were seeded at 10^6 cells in 75cm^2 flasks and cultured in the presence / absence of CET (5µg/ml) for 48h before being detached, washed twice with ice-cold PBS, sedimented and frozen in liquid nitrogen. Cell lysis as well as liquid chromatography tandem mass-spectrometric (LC-MS/MS) proteomic analysis were performed by Dr. Anna Jarzab (Chair of Proteomics, Technical University Munich).

For Western blot analysis, cells were washed twice in ice-cold PBS, lysed in RIPA buffer (Cell Signaling Technology, Danvers, MA, USA) supplemented with protease and phosphatase inhibitors (Roche Life Science, Penzberg, Germany) and scraped to facilitate cell detachment. Lysates were cleared by centrifugation at 105×g for 45 min at 4°C. Protein concentration was determined by Bradford assay: 2µl cleared protein lysate were added to 98µl diluted (1:50) Protein Assay Dye (Bio-Rad Laboratories Inc., Hercules, CA, USA). Absorption was measured using a Varioskan photometer (Thermo Fisher Scientific) at 595nm and compared to a reference curve generated with serial dilutions of bovine serum albumin (BSA) (Bradford, 1976).

LC-MS/MS analysis

LC-MS/MS analysis was performed at the Chair of Proteomics of the Technical University Munich. A detailed protocol written by Dr. Anna Jarzab can be found in *8.1 Attachment 1: Supplementary materials and methods*.

Data analysis

For statistical analysis, the LC-MS/MS results were imported into Perseus (v.1.5.4.1) (Tyanova et al., 2016). Samples from both resistant cell lines were grouped and compared to their parental counterpart (Lim1215 vs Lim1215-R and DiFi vs DiFi-R). A permutation based false discovery rate (FDR) adjusted two-sided Student's *t* test was used to assess statistically significant differences in protein expression and phosphorylation (FDR<0,05, S0 of 0,1). Proteins were annotated within Perseus with KEGG (Kyoto Encyclopedia of Genes and Genomes) annotations (Kanehisa & Goto, 2000). Phosphosites were annotated within Perseus with kinase-substrate annotation data (Hornbeck et al., 2015). Significantly overexpressed and depleted proteins were subjected to annotation enrichment analysis of KEGG pathways the STRING database (Szklarczyk et al., 2017). Kinase-substrate motifs of significantly overphosphorylated proteins and depleted phosphoproteins were subjected to annotation enrichment analysis of KEGG pathways using Perseus (Tyanova et al., 2016).

Western blotting

Protein expression analysis was also performed using Western blotting. 10µg of cell lysate generated during cell culture experiments were boiled in Lämmli buffer at a ratio of 4:1 for 10min at 95°C. Lysates were separated by sodium dodecyl sulfate polyacrylamide gel electrophoresis (SDS-PAGE) on 10% SDS-polyacrylamide gels (Table 3.1) for approximately 120min at 100V and transferred onto 0,2µm poly-vinylidene difluoride (PVDF) membranes (Bio-Rad) using the box blotting technique (XCell II™ Blot Module, Invitrogen, Carlsbad, CA, USA) at 100V for 60min. Membranes were blocked using 5% non-fatty milk powder in TBS-T (0,1% Tween 20) for 1h and incubated overnight under agitation at 4°C with primary antibodies. Membranes were washed with PBS and incubated under agitation with secondary antibodies for 1h at room temperature (RT). Finally, membranes were washed with PBS, submerged in chemoluminescent reagent (HRP substrate, Millipore, Burlington, MA, USA), visualised and quantified using a LI-COR Odyssey FC Scanner (Li-Cor, Lincoln, NE, USA) in combination with Image Studio (v.5.2). Refer to Table 2.4 in the *2. Materials* section for detailed composition of the Lämmli buffer, SDS-PAGE separating buffer, transfer buffer, TBS-T buffer and to Table 2.7 for antibody references.

Table 3.1: SDS-PAGE gel mix

	H_20	Tris base	10% SDS	30% acrylamide	APS	TEMED	Total volume
Seperation gel	3,96 ml	2,5 ml 1,5M, pH 8,8	100 µl	3,34 ml	100 µl	4 µl	10 ml
Stacking gel	1,36 ml	250 µl 1M, pH 6,8	20 µl	340 µl	20 µl	2 µl	2 ml

3.3 FUNCTIONAL ASSAYS

Transfection of small interfering RNA

EPH receptor A2 (*EPHA2*) gene knock-down was performed by Johanna Albert, M.Sc., as described previously using small interfering RNA (siRNA) (Albert, 2019). In short, cells were seeded at $8x10^5$ cells in $25cm^2$ flasks 24h before transfection. siRNA and Lipofectamine RNAiMAX (Thermo Fisher Scientific) were diluted in serum-free medium (OPTI-MEM, Thermo Fisher Scientific) and applied with fresh medium to cells, as detailed in the manufacturer's instructions. Cells transfected with scrambled siRNA were used as controls. Cells were used for subsequent analyses 24h after transfection. Gene knock-down was confirmed by reverse transcription quantitative real-time PCR (RT-qPCR) and by Western blotting. Refer to Table 2.8 in the *2. Materials* section for siRNA target sequences and manufacturers.

Ephrin-A1-Fc treatment

In order to trigger EPHA2 ligand-dependant signalling, cells were stimulated using recombinant ephrin-A1-Fc chimera (ephrin-A1-Fc) or IgG1-Fc control (Fc) alone (R&D Systems, Minneapolis, MN, USA). Cells were seeded 24h prior to treatment. Fresh medium was supplemented with 0,1µg/ml ephrin-A1-Fc or Fc control. The assay was performed 24h after cell stimulation.

EPHA2-antibody treatment

The EPHA2-signalling axis was specifically targeted using anti-EPHA2 (α-EPHA2) antibody treatment. This was achieved using a commercially available polyclonal goat Western blotting antibody directed at the extracellular domain of EPHA2. Cells were seeded 24h prior to treatment and subsequently treated with the anti-EPHA2 (α-EPHA2, Biotechne, Minneapolis, MN, USA) or anti-GFP (α-GFP, green fluorescent protein, Biotechne) control antibodies at 5µg/ml. Cells were used in assays 24h after treatment. The antibody clone references can be found in Table 2.7 in the *2. Materials* section.

Migration assay

In order to test cellular migration, cells were submitted to migration assays using a Boyden chamber assay (Fig. 3.1) (Boyden, 1962). Pre-treated cells (*EPHA2* knock-down, ephrin-A1-Fc stimulation, antibody treatment) were seeded after 24h in

technical triplicates in Transwell® inserts (8µm pore diameter, Corning, Corning, NY, USA) at 1 x 10^5 cells/insert in low FBS medium. High FBS medium was used as a chemoattractant. FBS concentrations for the relevant medium can be found in Table 3.2. For functional experiments involving tyrosine kinase inhibition, ephrin-A1 stimulation or α-EPHA2 antibody treatment the chemoattracting medium (high FBS medium) was supplemented with dasatinib (300nM) / vehicle control, ephrin-A1-Fc / Fc (0,1µg/ml), or α-EPHA2 / α-GFP (5µg/ml) antibodies. Cells were fixed after 72h using 100% freezing-cold methanol (-20°C), stained with crystal violet blue for 10 minutes and washed three times in ddH_2O. Non-migrated cells were removed from the insert using cotton swabs. Three representative pictures were taken from each membrane using an Axiovert 25 Inverted Phase Contrast Fluorescent microscope (Carl Zeiss, Oberkochen, Germany) at 5x magnification. Cell density of crystal-violet stained cells was assessed using ImageJ (1.49v) by quantifying blue-violet pixels in each image (Schneider et al., 2012). Briefly, the colour threshold was selected to highlight blue-violet tones (hue: 150-200). For colour saturation and brightness standard values were used across all experiments (saturation: 60-255; brightness: 70-255). Surface areas larger than 500 pixel units were quantified in order to exclude incidentally stained pores in the background. The percentage area covered by blue-violet pixels was used to quantify migration rates. The mean percentage area of all three images taken from each membrane (and standard deviation) was used for statistical analysis. Migration data was analysed using an unpaired two-sided Student's t test using GraphPad Prism (v.8.2.1).

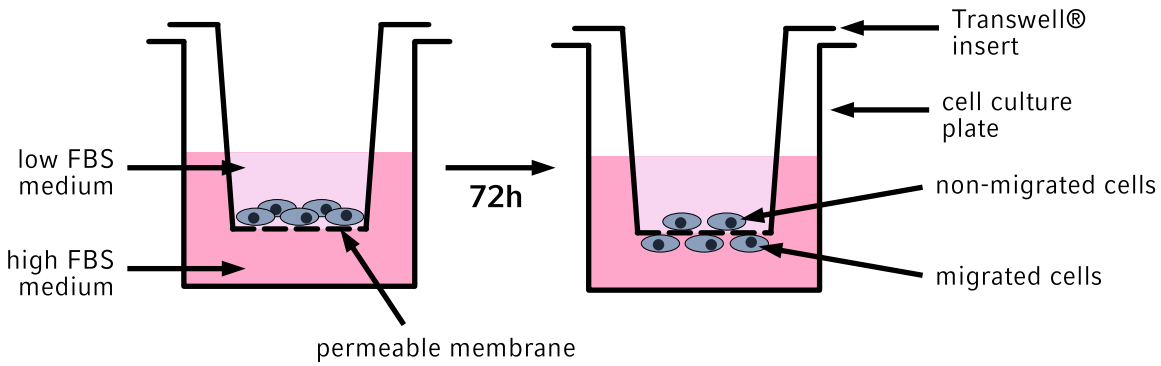

Figure 3.1: Schematic representation of a migration assay using a Boyden chamber.

Table 3.2: FBS concentrations used in migration assays

	Normal medium	Low FBS medium	High FBS medium
RPMI-1640 + 1% (v/v) pen/strep + 1µg/ml recomb. insulin	+ 5% (v/v) FBS	+ 0,25% (v/v) FBS	+ 10% (v/v) FBS
DMEM/Ham F-12 + 1% (v/v) pen/strep	+ 10% (v/v) FBS	+ 0,5% (v/v) FBS	+ 20% (v/v) FBS

Cell viability assay

Drug sensitivity for cetuximab and dasatinib (MedChemExpress, Monmouth Junction, NJ, USA) was measured by treating each cell line with increasing concentrations of the drug. Cells were seeded in tetraplicates at 3-4 x10^3 cells per well in a 96-well plate. Drugs or vehicle control were added 24h later at increasing concentrations. For drug sensitivity experiments cells were treated for 48h (CET) or 72h (dasatinib), for combination dasatinib and cetuximab treatment cells were treated for 72h. Viability was assessed by adding 10µl alamarBlue™ reagent (Thermo Fisher Scientific) to each well and measuring fluorescence after 4h using a Varioskan plate reader (Thermo Fisher Scientific). Cell viability and half maximal inhibitory concentrations (IC_{50}) were assessed using GraphPad Prism (v.8.2.1).

3.4 RNA EXTRACTION, RT-PCR AND RT-QPCR

Cellular RNA extraction and reverse transcription quantitative real-time PCR (RT-qPCR) were described in detail elsewhere (Albert, 2019). In short, cells were washed twice in ice-cold PBS prior to RNA extraction. Cells were scraped to facilitate detachment and RNA was isolated using RNeasy Mini Kits according to the manufacturer's instructions. Reverse transcription PCR (RT-PCR) was performed with 1µg RNA using RevertAid Reverse Transcriptase and random hexamer primers according to the manufacturer's instructions (Thermo Fisher Scientific). The RT-PCR reaction mix protocol can be found in Table 3.3 and was prepared on ice. RT-PCR was performed in a thermal cycler at 25°C for 10min, followed by an elongation phase of 60min at 42°C. The reaction was inactivated at 70°C for 10min. Complementary DNA (cDNA) samples were stored at -20°C.

Table 3.3: RT-PCR reaction mix

Reagent	Volume
5x Reaction Buffer®	8µl
RiboLock RNase Inhibitor®	1µl
dNTP mix (10mM)	4µl
Random hexamer primers	2µl
RevertAid® reverse transcriptase	2µl
RNA	1000µg
RNase-free water	*ad* 40µl
Total volume	40µl

For analysis of gene expression levels, RT-qPCR was performed using the Universal ProbeLibrary system (UPL) with Probes Master reagents and gene specific primers according to the manufacturer's instructions (Roche Life Science). Detailed instructions for the RT-qPCR reaction mix can be found in Table 3.4, gene specific primers and UPLs are listed in Table 2.9 in the *2. Materials* section. RT-qPCR reactions were performed in technical triplicates in sealed plates using a RT-qPCR Mastercycler (Bio-Rad) following the protocol in Table 3.5. Gene expression levels

were calculated applying the ΔΔCt method thereby normalising to GAPDH expression levels (Pfaffl, 2006):

ΔCt = Ct(gene of interest) – Ct(housekeeping gene)

ΔΔCt = ΔCt(sample) – ΔCt(control)

Fold change = $2^{-\Delta\Delta Ct}$

Table 3.4: RT-qPCR reaction mix

Reagent	Volume
Roche Probe Master®	5µl
Forward primer (500nM)	0,05µl
Reverse primer (500nM	0,05µl
UPL	0,1µl
cDNA	2µl
DNase-free water	*ad* 10µl
Total volume	10µl

Table 3.5: RT-qPCR reaction protocol

Reaction	Temperature	Time	Cycles
Preincubation	95°C	10 min	1
Amplification	95°C	10 sec	40
	60°C	15 sec	
Cooling	40°C	30 sec	1

3.5 Clinical and transcriptomic data

Patients and samples

This study made use of previously published clinical and transcriptomic datasets (Heinemann et al., 2014; Roessler et al., 2015; Sayagués et al., 2016; Stintzing et al., 2012; Woolston et al., 2019). All clinical data used were generated in accordance with the relevant study protocol, in compliance with the Declaration of Helsinki and were approved by an ethics committee.

Patient recruitment for the FIRE-3 trial has been described elsewhere (https://clinicaltrials.gov/; trial number NCT00433927; Heinemann et al., 2014; Stintzing et al., 2012). Before an amendment excluded patients with *RAS* and *RAF* alterations from the trial, 211 patients were recruited and randomised for cetuximab treatment regardless of their *RAS* status. 187 (84%) of these patients (130 *RAS* wildtype and 57 *RAS* mutated) were included here in order to assess *EPHA2* expression and outcome in the context of primary CET resistance.

Patient recruitment for the Prospect-C trial has been described elsewhere (https://clinicaltrials.gov/; trial number NCT02994888; Woolston et al., 2019). Patients with mCRC received a baseline (BL) tissue biopsy before being treated with

single-agent CET. Patients with progressive disease as defined by RESIST v1.1 criteria later received a progressive disease (PD) tissue biopsy (Eisenhauer et al., 2009). Patients were classified according to the response to single-agent CET treatment into patients with primary progression and with prolonged treatment benefit: primary disease progression was defined as disease progression before or at the first computed tomography scan (at 12 weeks), all other patients were considered to show prolonged benefit. Of the 46 patients originally recruited for single-agent CET treatment, 3 (7%) were included here in order to assess *EPHA2* expression and outcome in the context of acquired CET resistance in mCRC patients (Figure 4.19A).

Genomic and transcriptomic analyses

Tumour samples from the FIRE-3 trial were probed for mutations by pyrosequencing for the following oncogenes: *KRAS* exons 2 (codons 12 & 13), 3 (codon 61) and 4 (codon 146), *NRAS* exons 2 (codon 12 & 13), 3 (codons 56 & 61) and 4 (codons 117 & 146) as well as *BRAF* exon 15 (codon 600) mutations.

Tissue biopsy samples from the Prospect-C trial were subjected to exome sequencing and DNA copy number variation analysis, as described previously (Woolston et al., 2019).

Transcriptomic data

Gene expression data from tumour samples collected in the FIRE-3 trial were generated by ALMAC® using a modified Affymetrix Xcel™ gene expression array. Gene expression data from BL and PD biopsies within the Prospect-C trial were generated as described previously (Woolston et al., 2019). Separately, in order to assess *EPHA2* expression in the context of metastasis, expression data from 2 published microarray datasets comprising a total of 25 patients with mCRC (UICC IV) were downloaded from the Gene Expression Omnibus database (https://www.ncbi.nlm.nih.gov/geo/; GEO accession GSE40367 & GSE81582) (Barrett et al., 2013; Roessler et al., 2015; Sayagués et al., 2016).

Statistical analysis and survival data

Survival curves were plotted using the Kaplan-Meier method and significance tested using the log-rank test. Objective response rate (ORR) was defined according to RECIST v1.1 criteria (Eisenhauer et al., 2009). The *EPHA2* expression cut-off value separating $EPHA2_{high}$ and $EPHA2_{low}$ tumours was generated using the median gene expression level across all samples. Survival analysis was performed with GraphPad Prism (v.8.2.1) and statistical significance was considered achieved for p values <0,05 (two-sided).

4 RESULTS

4.1 LC-MS/MS BASED PROTEOMICS CHARACTERISE CETUXIMAB RESISTANT COLORECTAL CELL LINES

In order to uncover molecular drivers of *KRAS* associated cetuximab (CET) resistance this study used a well-established cell culture model of acquired CET resistance kindly provided by Dr. Alberto Bardelli (Candiolo Cancer Institute, Italy) (Misale et al., 2012). Two pairs of isogenic CET resistant cell lines (Lim1215 R1, Lim1215 R2, DiFi R1 and DiFi R2) were independently derived from CET sensitive parental Lim1215 and DiFi cell lines by long-term treatment with CET. In all four resistant cell lines, CET resistance was conferred by activating *KRAS* mutations (Lim1215 R1, Lim1215 R2) or *KRAS* amplification (DiFi R1, DiFi R2).

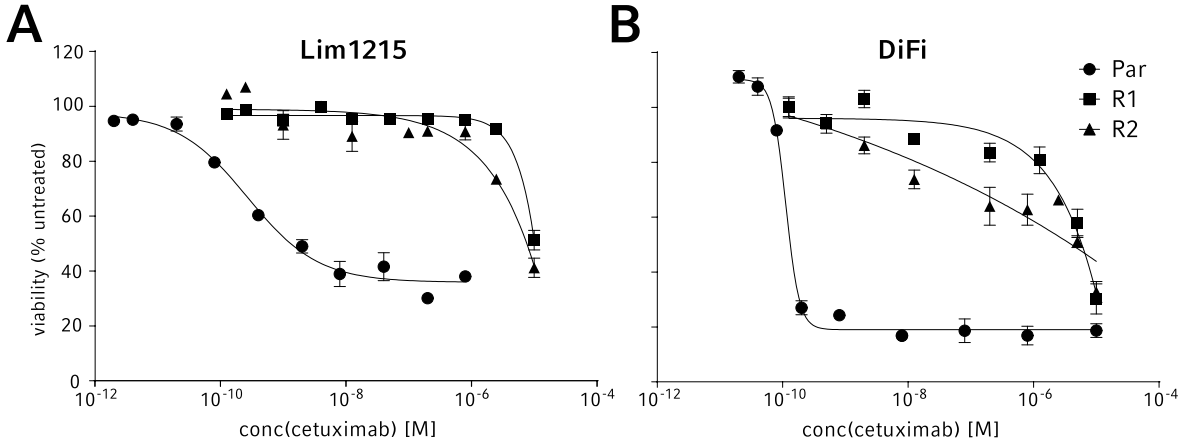

Figure 4.1: Sensitivity of parental and resistant cell lines to cetuximab. **(A)** Lim1215 and **(B)** DiFi, parental (Par) and resistant cell lines (R1 & R2) were treated for 48h with increasing doses of cetuximab. Viability was measured using alamarBlue® reagent. Respectively representative of three experiments. Graphed data represents mean relative viability (compared to untreated) ± SEM of three technical replicates.

In order to confirm cell line identity and drug resistance, short tandem repeat (STR) profiling, Next-Generation Sequencing (NGS) and cetuximab sensitivity measurement (IC_{50}) were performed. STR-profiling and NGS confirmed cell line authenticity and *KRAS* mutational status. Cell viability assay confirmed CET sensitivity in Lim1215 and DiFi cell lines as well as CET resistance in all four resistant cell lines (Table 4.1, Fig. 4.1).

cell line	cell line identity score	chrom. pos.	gene	cDNA	type	exon	Ref. mRNA	Protein	Cov.	CNV (fold)	AF	clinical significance
Lim1215	100%	chr3:41266124	CTNNB1	c.121A>G	SNV	3	NM_001904.3	p.Thr41Ala	1997		100	path, lik path
		chr15:66774159	MAP2K1	c.635G>A	SNV	6	NM_002755.3	p.Ser212Asn	1997		100	prob path
Lim1215 R1	93,75%	chr3:41266124	CTNNB1	c.121A>G	SNV	3	NM_001904.3	p.Thr41Ala	1739		100	path, lik path
		chr12:25398285	KRAS	c.34G>C	SNV	2	NM_033360.3	p.Gly12Arg	1607		49.41	path
		chr15:66774159	MAP2K1	c.635G>A	SNV	6	NM_002755.3	p.Ser212Asn	1997		100	prob path
Lim1215 R2	93,33%	chr3:41266124	CTNNB1	c.121A>G	SNV	3	NM_001904.3	p.Thr41Ala	736		100	path, lik path
		chr12:25398281	KRAS	c.38G>A	SNV	2	NM_033360.3	p.Gly13Asp	980		50.51	path, lik path
		chr15:66774159	MAP2K1	c.635G>A	SNV	6	NM_002755.3	p.Ser212Asn	1346		100	prob path
DiFi	96,55%	chr7:55198955	EGFR		CNV					10,7		path, lik path
DiFi R1	96,55%	chr7:55198955	EGFR		CNV					6,7		path, lik path
		chr12:25364760	KRAS		CNV					21,7		path, lik path
DiFi R2	96,55%	chr7:55198955	EGFR		CNV					6,7		path, lik path
		chr12:25364760	KRAS		CNV					28,7		path, lik path

Table 4.1: Short Tandem Repeat and Next Generation Sequencing results (Oncomine Focus Assay)

Cell line identity score, short tandem repeat profile allele overlap (%); **AF**, allele frequency; **cDNA**, complementary DNA; **CNV**, copy number variation; **Cov.**, Coverage; **lik path**, likely pathogenic; **path**, pathogenic; **prob path**, probably pathogenic (based on prediction algorithms, no information in ClinVar); **SNV**, single nucleotide variant

Having confirmed the reliability of the cell culture model, a proteomic approach was selected in order to uncover downstream molecular effects of overactive KRAS signalling in the resistant Lim1215 (Lim1215-R) and DiFi (DiFi-R) cell lines. Biological triplicates for each parental and resistant cell lines were either treated with cetuximab (5µg/ml) or left untreated for 48h. Cells were frozen in liquid nitrogen and processed for mass-spectrometric proteomic analysis at the Chair of Proteomics of the Technical University, Munich (Fig. 4.2). Mass-spectrometric based proteomics successfully identified and quantified approximately 7000 proteins and over 1000 phosphorylation sites (phosphosites) in all parental and resistant cell lines.

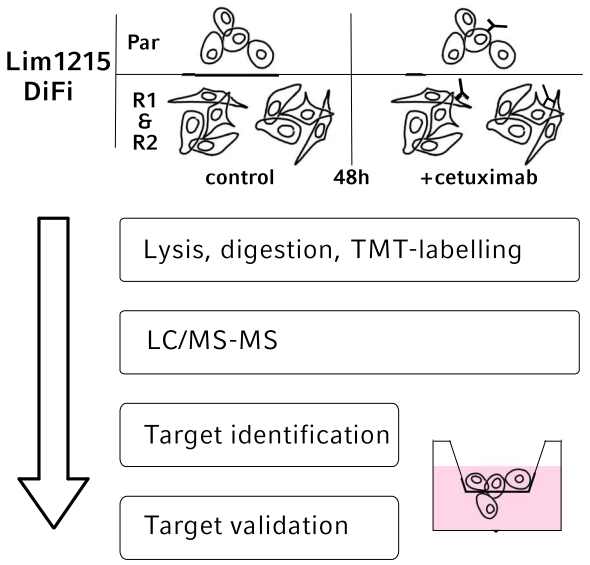

Figure 4.2: Experimental design of liquid chromatography tandem mass-spectrometry (LC/MS-MS) based characterisation of CET resistance in Lim1215 & DiFi cell lines.

The technical quality of both the proteomic and the phosphoproteomic data was assessed by correlating the data from individual replicates with one another in scatter plots and by performing principal component analyses (PCA). Biological replicates displayed excellent correlation of their protein expression data (Pearson's R>0,98; Fig. 4.3A-D). This was also true for the phosphoproteomic data, despite the lower correlation between biological replicates (Pearson's R>0,95; Fig. 4.3E-H), most likely caused by a generally higher variance in protein phosphorylation than in protein expression within biological replicates. Principal component analysis is a widely used technique that reduces the dimensionality of complex datasets by finding variables that maximise variance within the dataset (Jollife & Cadima, 2016). PCAs of proteomic and phosphoproteomic data showed a solid clustering of individual samples by biological replicate rather than by experimental replicate (Fig. 4.4A-B). Additionally, samples from resistant cell lines clustered more closely to one another than to their respective parental counterpart. This indicates that despite having been established completely independently resistant cell lines share similar patterns of protein expression and phosphorylation when compared to their parental counterparts. Taken together, the results from the correlation analysis and the PCAs supports the technical quality of the data and indicates a similar biology throughout the resistant cell lines despite having been generated independently.

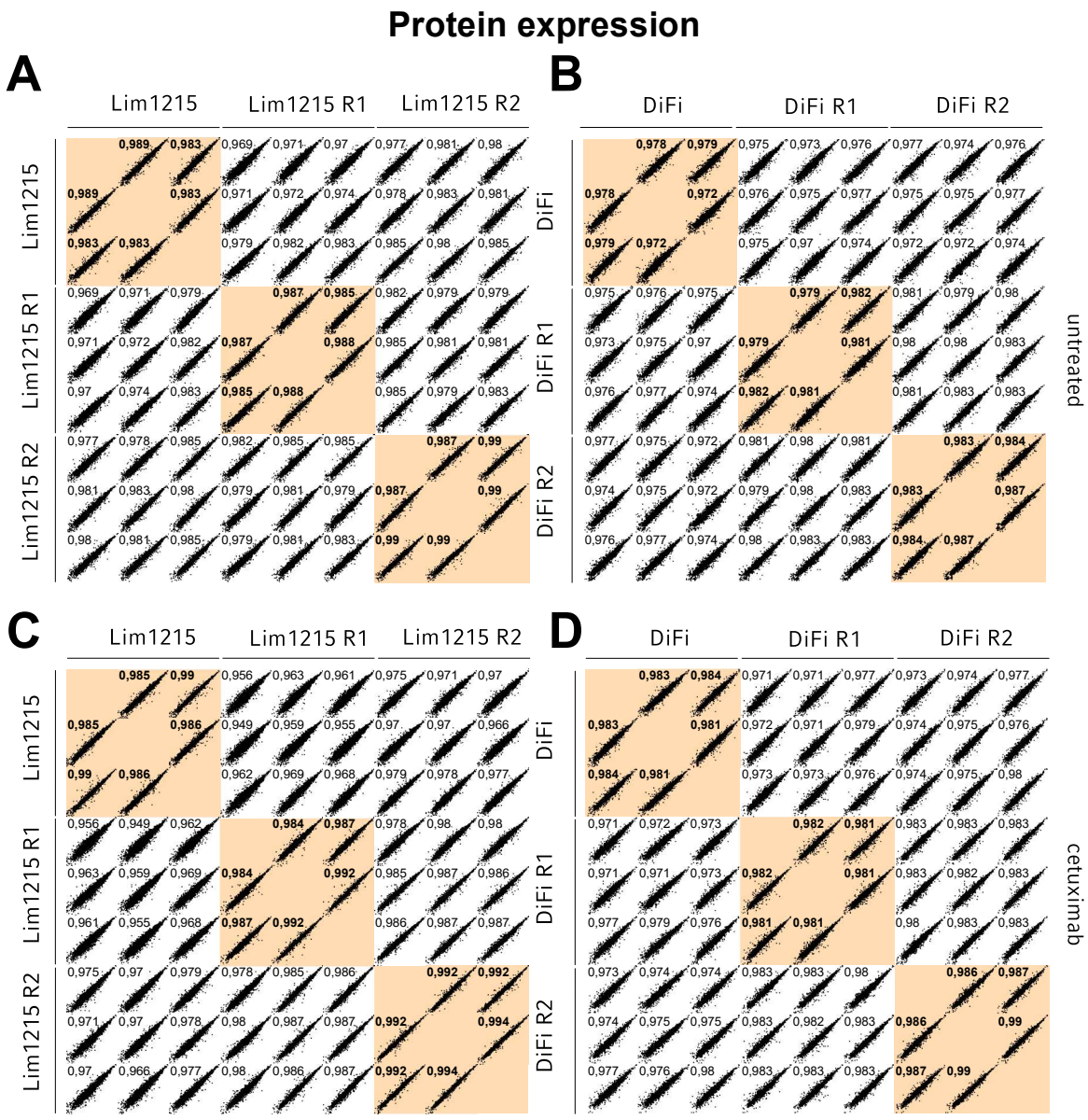

Figure 4.3: Scatter plots display the correlation of protein expression data **(A - D)** and protein phosphorylation **(E - H)** between each of the samples and associated Pearson R. Individual replicates of Lim1215 **(A, C, E, G)** and DiFi cell lines **(B, D, F, H)** show an excellent correlation of protein expression data (Pearson R > 0,98) and a solid correlation of protein phosphorylation patterns (Pearson R > 0,95) according to the experimental setting (untreated **A, B, E, F**; cetuximab **C, D, G, H**).

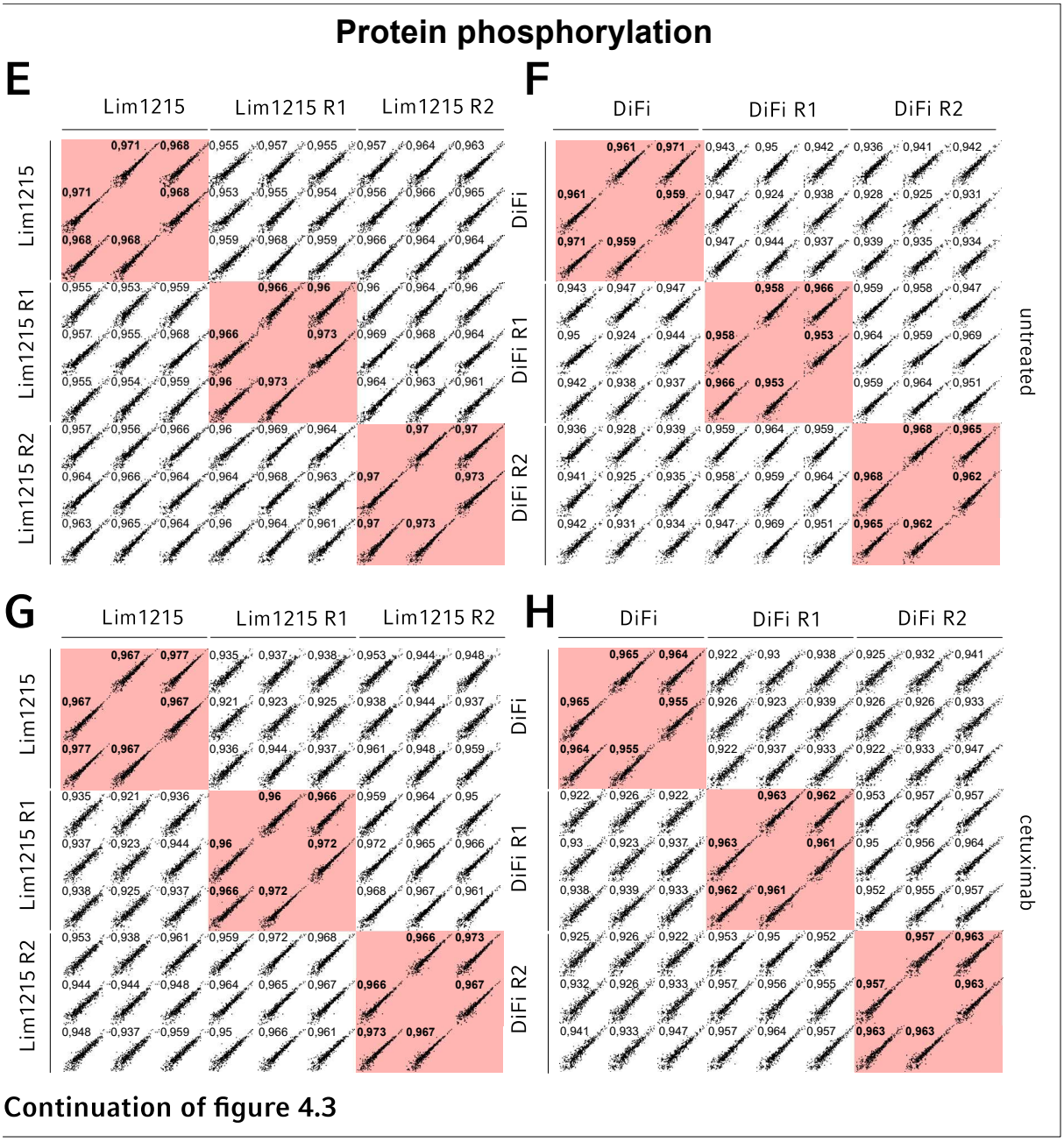

Continuation of figure 4.3

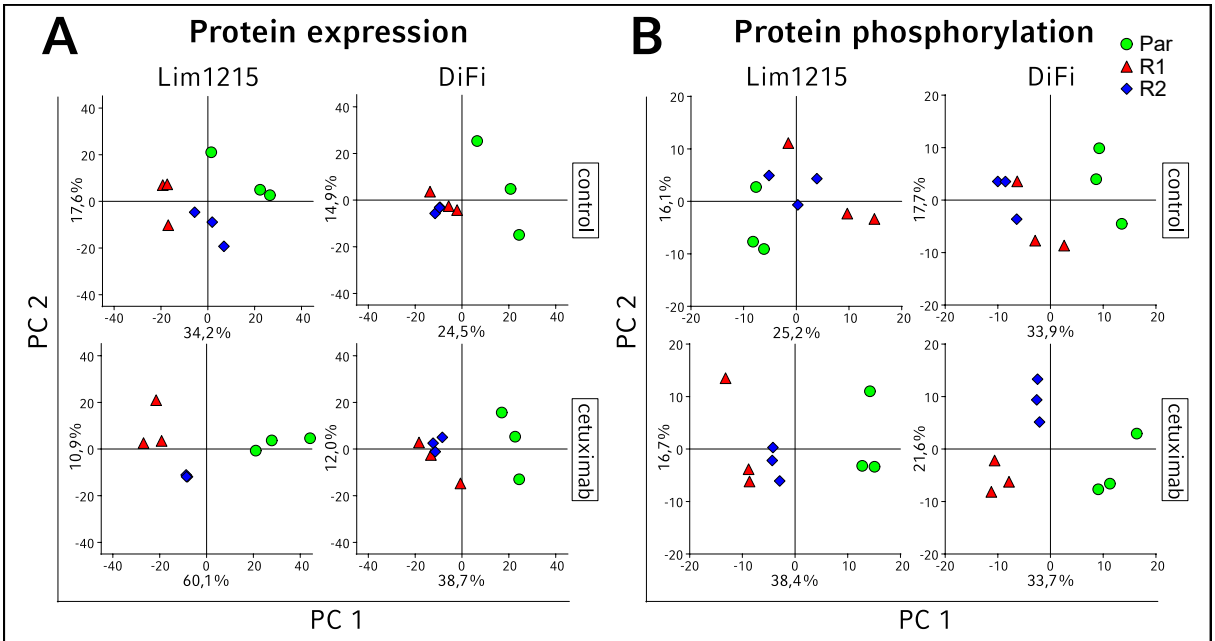

Figure 4.4: Principal component analyses of proteomic **(A)** and phosphoproteomic data **(B)** show solid clustering of biological replicates together as opposed to clustering by experimental replicate. In both protein expression **(A)** and protein phosphorylation data **(B),** both resistant cell lines cluster more tightly compared to their parental counterpart. Par: Parental cell line; R1: Lim1215-R1 / DiFi-R1; R2: Lim1215-R2 / DiFi-R2.

4.2 Chemical proteomics confirm cetuximab mode of action

After having been assessed for technical reliability, the mass-spectrometric data was next assessed for biological reliability by using the expected CET mode of action in sensitive parental cell lines. CET treated and untreated parental Lim1215 and DiFi cell lines were compared for protein expression and phosphorylation changes induced by antibody treatment. Changes in protein expression or phosphorylation were uncovered using a two-sided FDR controlled *t* test (FDR<0,05; S0 of 0,1). The biological effects of the antibody treatment were identified by performing unsupervised hierarchical clustering of the significantly changing (phospho)proteins in order to separate them into overexpressed and depleted (phospho)proteins under CET treatment (Fig. 4.5A-B). The biological effects of CET treatment were highlighted by performing enrichment analysis of protein KEGG annotations (Kyoto Encyclopedia of Genes and Genomes; Kanehisa & Goto, 2000) and kinase-substrate motifs annotation using the STRING database and Perseus respectively (Szklarczyk et al., 2017; Tyanova et al., 2016). Enrichment of kinase-substrate (phosphorylation) motifs within the phosphoproteomic data was used to infer changes in kinase activity upstream of specific phosphosites.

Changes in protein expression were marked by a depletion of proteins associated with the cell division cycle in both CET treated Lim1215 and DiFi cell lines ($FDR_{Lim1215}$=5,70 x 10^{-4}; FDR_{DiFi}=1,48 x 10^{-2}) (Fig. 4.5A). This was reflected by the depletion of key cell cycle proteins such as the Myc proto-oncogene protein (MYC), cyclins and cyclin dependent kinases (G1/S-specific cyclin-D1, CCND1; cyclin-A2, CCNA2; cyclin-H, CCNH; cyclin-dependent kinase 2, CDK2), mitogen-activated protein kinase 14 (MAPK14) as well as epidermal growth factor receptor (EGFR) in DiFi. This concurs with the well-known mechanism of action of CET, which causes EGFR-internalisation and degradation (Okada et al., 2017; Vincenzi et al., 2010). Other signalling pathways beside the cell division cycle were affected by CET treatment. Treated Lim1215 cells were characterised by a depletion in proteins associated with the metabolic- ($FDR_{LIM1215}$=3,03 x 10^{-10}) and AMPK- ($FDR_{LIM1215}$=3,58 x 10^{-2}) signalling pathways. This effect on metabolic signalling was illustrated by depletion of phosphatidylinositol 4,5-bisphosphate 3-kinase catalytic subunit alpha isoform (PIK3CA) and RAC-alpha serine/threonine-protein kinase (AKT1) in treated cells, which also concurs with previously described CET mechanisms of action (Scott et al., 1998; Thomas et al., 2002; Vincenzi et al., 2010). In treated DiFi cells the mismatch repair- (FDR_{DiFi}=6,70 x 10^{-3}) and nucleotide excision repair (FDR_{DiFi}=6,70 x 10^{-3}) signalling pathways were depleted. Interestingly, no overexpressed pathways could be identified in either parental cell line when treated with CET.

Changes in protein phosphorylation and subsequent enrichment analysis of over-phosphorylated or dephosphorylated phosphosites yielded few pathways affected by CET treatment (Fig. 4.5B). Additionally, none of the enriched pathways reached significant enrichment, making the interpretation of these results difficult.

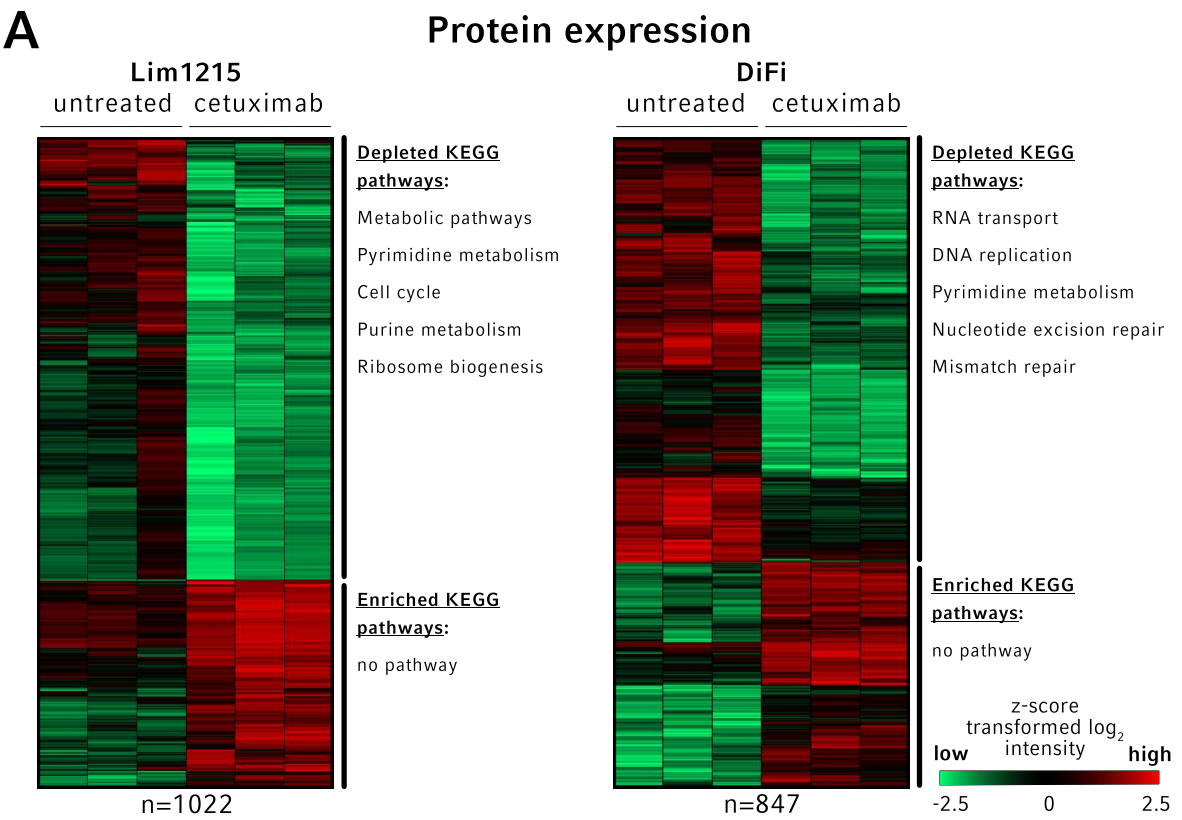

Figure 4.5: LC-MS/MS based proteomic characterisation of cetuximab (CET) mode of action. **(A)** Unsupervised clustering of significant protein expression changes upon CET treatment and KEGG annotation enrichment analysis in parental Lim1215 and DiFi cells. KEGG annotation enrichment analysis using the STRING database yielded several pathways depleted by CET (graph features 5 most depleted pathways in each cell line). Enrichment analysis did not yield any pathways enriched by CET treatment. **(B)** Unsupervised clustering of significant protein phosphorylation changes upon CET treatment and enrichment of kinase-substrate motifs in parental Lim1215 and DiFi cells. Kinase-substrate motifs enriched using Perseus show enrichment of kinase activity, however without reaching significance (n.s.: non-significant). Log_2 expression intensities were z-score transformed (Bejamini-Hochberg-FDR=0,05; S0=0,1).

Taken together, these results validate the biological reliability of the mass-spectrometric dataset by identifying known mechanisms of action of CET treatment within the proteomic datasets. The biological reliability of the phosphoproteomic dataset could not be confirmed. This is almost certainly due to the low identification count of phosphosites in the LC-MS/MS experiment. The phosphoproteomic data was therefore interpreted with caution in the subsequent analyses.

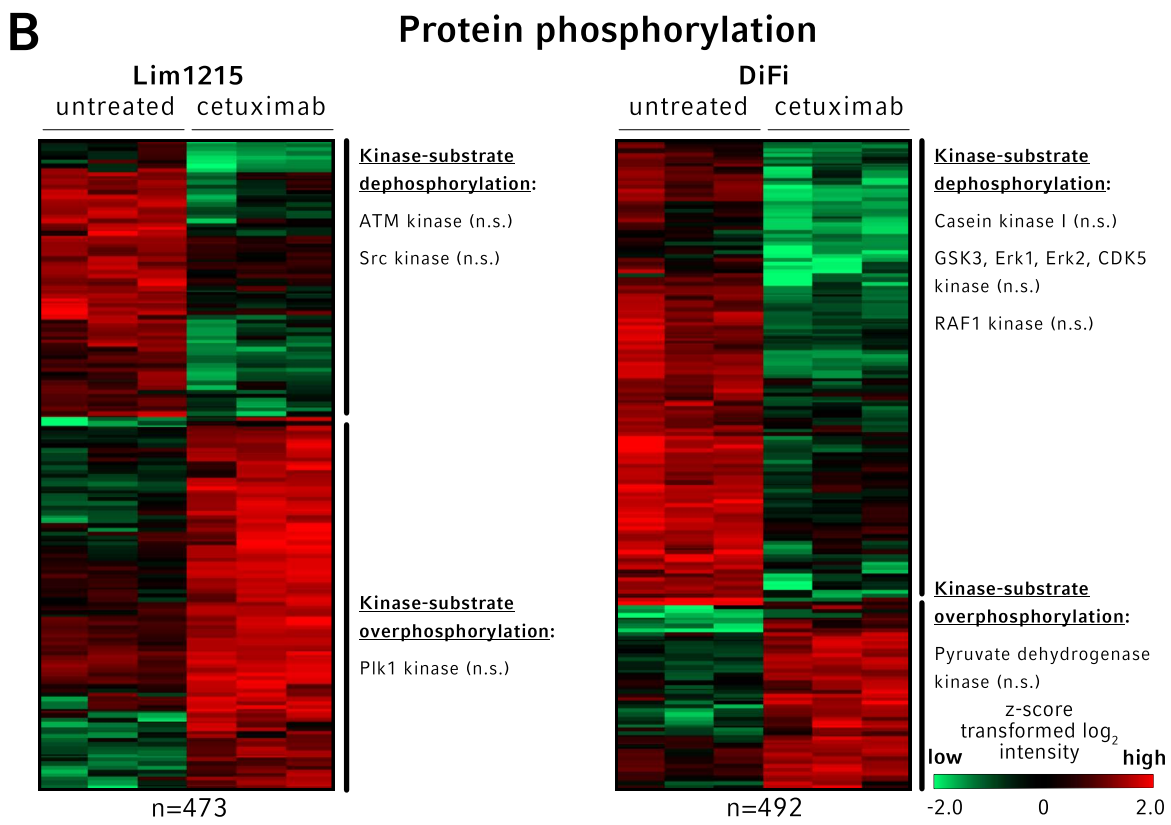

Continuation of figure 4.5

4.3 Resistant cells differ from parental cells in their response to treatment

After validating the technical and biological reliability of the data CET resistant cells were probed for protein expression and phosphorylation changes linked to CET resistance. In Lim1215 and DiFi, both resistant cell lines were jointly compared to their parental counterpart (e.g. Lim1215-R1 & Lim1215-R2 compared to Lim1215) in search of overlapping molecular signatures (FDR controlled *t* test, FDR<0,05; S0 of 0,1).

Within the proteomic dataset protein expression levels differed little when comparing resistant and parental cells in the untreated setting, and resistance accounted for significant expression differences in only 2.4% (Lim1215) and 3.0% (DiFi) of all identified proteins. However, when treated with CET, resistant and parental cell lines displayed significant protein expression changes in 53.3% and 23.3% of identified proteins for Lim1215 and DiFi respectively (Fig 4.6A-B).

This was also reflected by protein phosphorylation, where resistant cells mainly differed from their parental counterparts in the CET treated setting (Fig. 4.6C-D). Untreated Lim1215-R cells displayed phosphorylation differences in less than 1% of identified phosphosites compared to 22% in the treated setting. Interestingly, DiFi-R cells showed little phosphorylation differences to their parental counterparts, and this did not change much upon CET treatment (12% difference in untreated cells; 11%

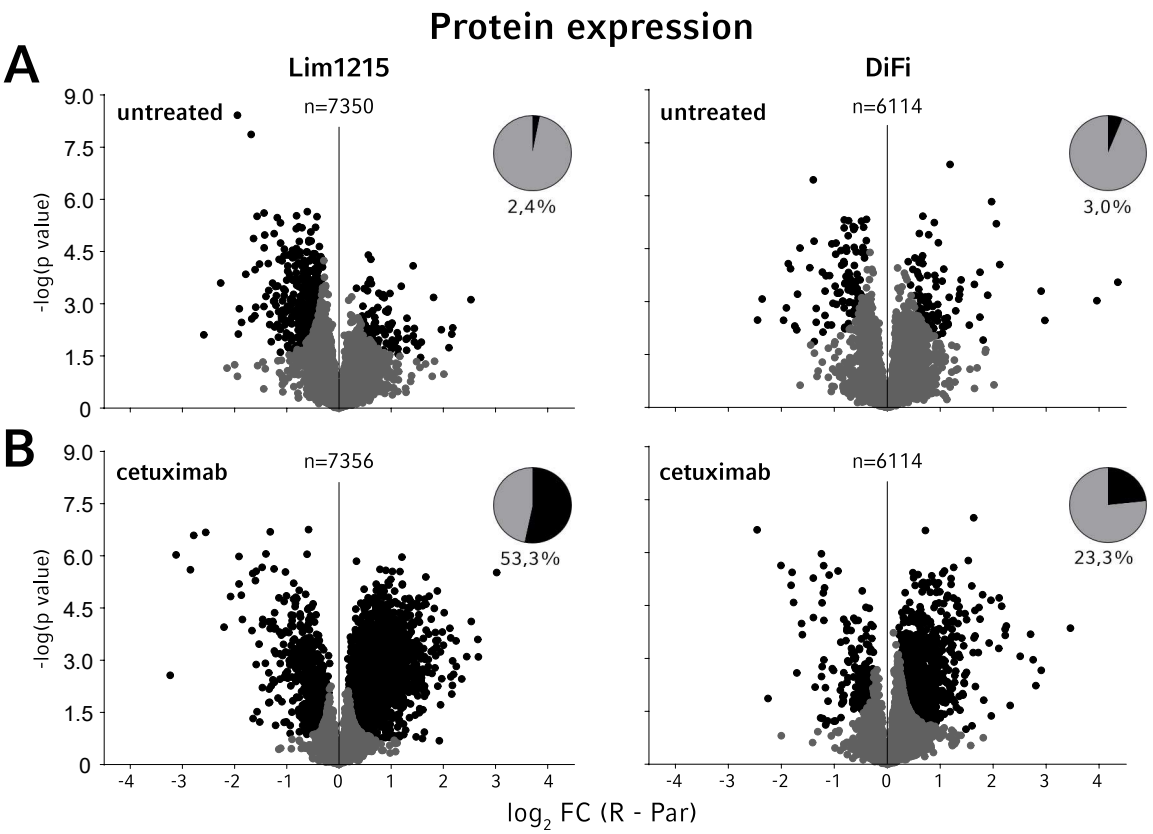

Figure 4.6: LC-MS/MS based proteomics identifies treatment dependent differences between resistant and parental cell lines. Volcano plots of changes in protein expression **(A, B)** and protein phosphorylation **(C, D)** in resistant cells compared to parental cells. Expression differences were plotted as $\log_2$ fold-change (FC) against the significance of the difference (FDR<0.05; S0 of 0,1; black dots). Both resistant cell lines (R) were jointly compared to their parental counterpart (Par) in the untreated **(A, C)** and CET treated **(B, D)** state.

in CET treated cells). This is however biased by the low phosphosite count acquired during the LC-MS/MS experiment.

These results indicate most proteomic and phosphoproteomic differences between resistant and parental cell lines to be mainly reactional to CET treatment rather than intrinsic.

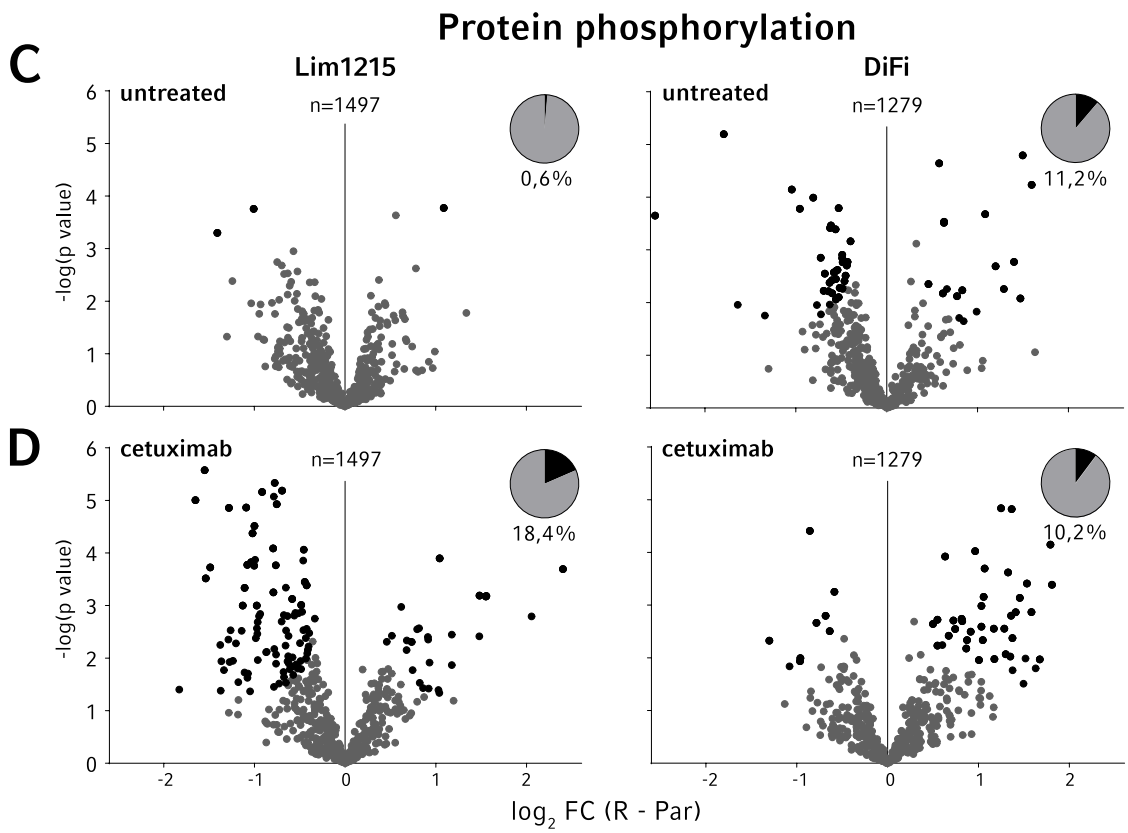

Continuation of figure 4.6

4.4 KINOME REPROGRAMMING IN RESISTANT CELL LINES IS CHARACTERISED BY EPHA2 OVEREXPRESSION

In an attempt to reveal changes in cellular signalling in resistant cells, enrichment analysis of significantly overexpressed proteins and phosphoproteins was performed. As indicated above resistant cell lines seemed to differ from their parental counterpart through their reaction to CET treatment. In order to further define this reaction to CET, a focus was set on protein expression and phosphorylation differences between resistant and parental cell lines in the CET treated setting.

In CET treated cells, enrichment analysis of overexpressed proteins using the STRING database showed an enrichment of ribosomal proteins (FDR=8,86 x 10^{-8}), ABC transporters (FDR=5,10 x 10^{-3}) and metabolic proteins (FDR=3,64 x 10^{-2}) in Lim1215-R cells, as well as an enrichment of DNA replication (FDR=8,50 x 10^{-4}), cell cycle (FDR=6,60 x 10^{-3}) and DNA mismatch repair proteins (FDR=1,12 x 10^{-2}) in DiFi-R cells (Fig 4.7A). This indicates that CET resistance has a large impact on a variety of cellular processes.

As mentioned previously protein kinases are key regulators of many cellular processes. Protein kinases regulate cell signalling both through changes in kinase activity and kinase expression (Blume-Jensen & Hunter, 2001; Fleuren et al., 2016). In order to uncover kinome reprogramming in resistant cells, kinase activity was

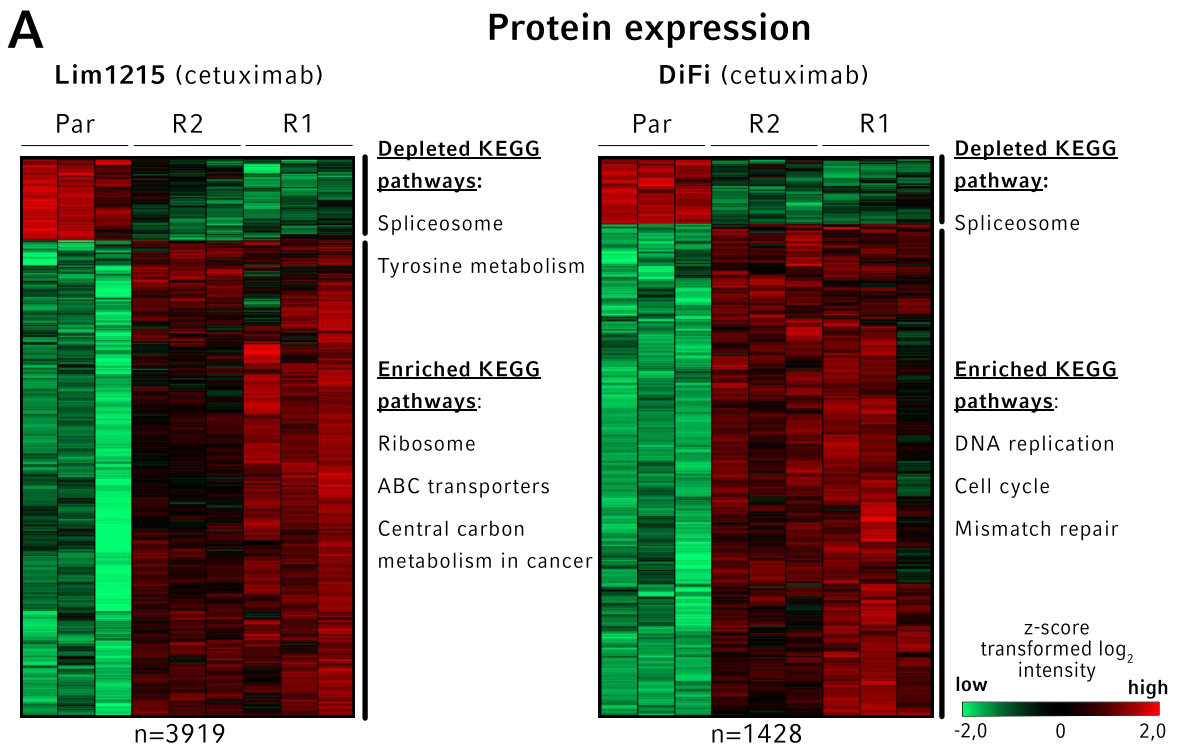

Figure 4.7: LC-MS/MS based proteomics identifies expression changes in pathways associated with hallmarks of cancer in CET resistant cell lines. **(A)** Unsupervised clustering and KEGG annotation enrichment analysis of significantly deregulated proteins in CET treated resistant Lim1215 and DiFi cells. Log_2 expression intensities of differentially expressed proteins were z-score transformed. KEGG term enrichment analysis using the STRING database show significant enrichment of various pathways associated with hallmarks of cancer in Lim1215-R and DiFi-R cell lines. **(B)** Unsupervised clustering and kinase-substrate motif enrichment analysis of significantly changing protein phosphorylation in Lim1215 and DiFi cells. Kinase-substrate motifs enriched using Perseus show enrichment of kinase activity, however without reaching significance (n.s.: non-significant).

inferred through kinase-substrate interaction analysis of phosphorylated proteins, whereas kinase expression was measured in the proteomics dataset.

Kinase activity within specific signalling pathways was inferred by kinase-substrate interactions analysis of downstream phosphorylated proteins. Enrichment analysis of kinase-substrate motif annotations in over- and dephosphorylated proteins using Perseus showed several enriched kinase-substrate motifs, though none of these reached significance (Fig. 4.7B). This is most undoubtedly due to the low identification count of phosphosites in the phosphoproteomic experiment. However, positive enrichment of Erk1/2 substrate motifs in both treated Lim1215-R and DiFi-R cell lines compared to the parental cell lines, despite being non-significant, may serve as a positive control within the dataset, as *KRAS* mutations/amplifications in resistant cell lines are expected to induce constitutively active MAPK-signalling, which induces

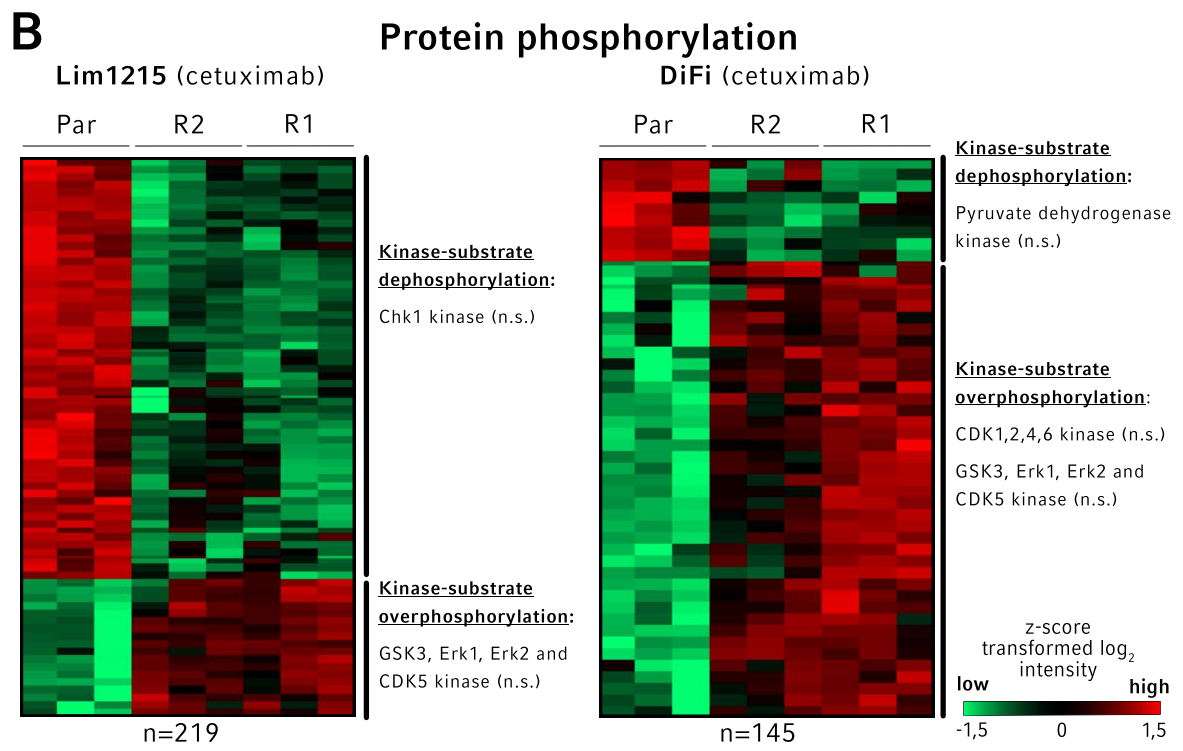

Continuation of figure 4.7

overphosphorylation of Erk1/2 targets (Fig. 4.7B). Undeniably the low phosphosite count in the dataset make the interpretation of these data difficult.

These results show no significant increase in kinase activity in the phosphoproteomic dataset, the interpretation of which is made difficult by the low quantity of data in the dataset.

As the analysis of kinase activity did not yield any overlapping features common to all resistant cell lines, protein kinase expression was selected for further analysis. Kinase expression is known to play a major role in kinome reprogramming and has been associated with drug resistance in other cancer entities (Fleuren et al., 2016; Koch et al., 2015; Ruprecht et al., 2017). In a first step, global kinase expression differences were identified using an FDR controlled t test (FDR<0,05; S0 of 0,1). In this approach, overall kinase expression changes were concordant with expression changes in the total proteome as described above. Untreated resistant cell lines showed little difference from parental cells in kinase expression (Lim1215: 6.3%; DiFi: 3.7%). These differences increased almost tenfold in the treated setting (Lim1215: 47%; DiFi: 35%). This shows kinase expression behaves similarly to total proteome changes in resistant cells and is dependent on exposure to CET (Fig 4.8).

In order to identify overexpressed kinases in resistant cells kinases were ranked by their log_2 fold expression change (log_2 FC) incurred by resistance (Fig. 4.9). Interestingly, many known oncoproteins were overexpressed in individual resistant cell lines. This included hepatocyte growth factor receptor (MET), PIK3CA, proto-oncogene tyrosine-protein kinase Src (SRC) and AKT1. Interestingly, ephrin type A

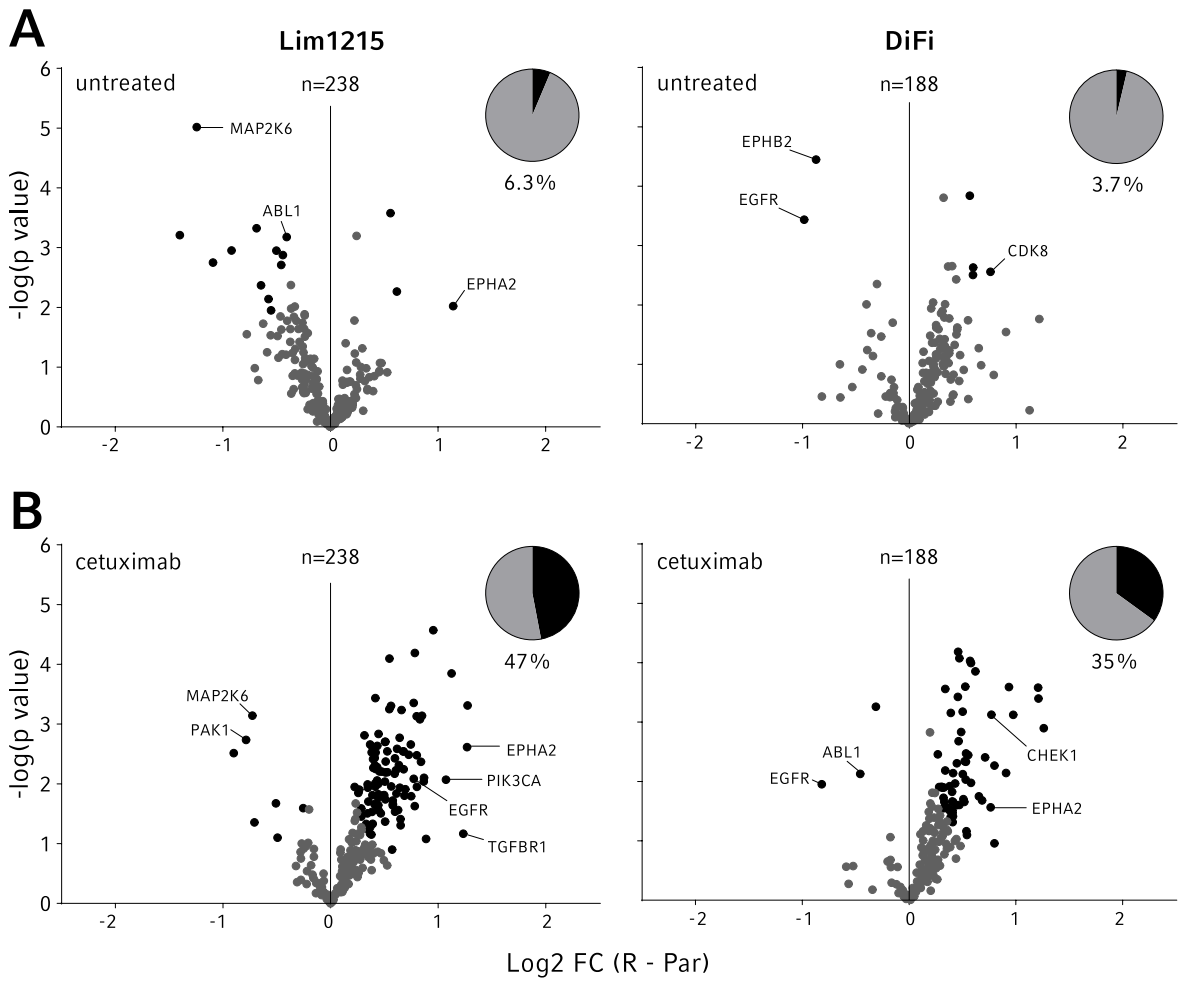

Figure 4.8: LC-MS/MS based proteomics identifies overexpressed kinases in resistant cell lines. **(A, B)** Volcano plots of protein kinase expression changes in resistant cells compared to parental cells. Expression differences were plotted as $\log_2$ fold-change (FC) against the significance of the difference (FDR<0,05; S0 of 0,1; black dots). Both resistant cell lines (R) were jointly compared to their parental counterpart (Par) in the untreated **(A)** and cetuximab treated **(B)** state.

receptor 2 (EPHA2) was among the most overexpressed kinases and unlike other mentioned oncoproteins was overexpressed in all four resistant cell lines.

EPHA2 is a 130kDa receptor tyrosine kinase of the EPH receptor family, the largest family of receptor tyrosine kinases and is encoded by the EPH receptor A2 (*EPHA2*) gene. EPH receptors, together with their membrane-bound ligands ephrins, regulate cellular signalling involved in the physiology of organogenesis, tissue compartment formation and angiogenesis amongst others by regulating short-distance cell-cell signalling (Kania & Klein, 2016) (Fig. 4.10A). Ephrin-EPH receptor signalling involves both forward and reverse signalling. Reverse signalling in characterised through signalling downstream of membrane bound ephrins that bind to EPH receptors. Forward signalling is characterised by signalling downstream of EPH receptors. Forward EPHA2 receptor signalling is dependent on ligand binding: ligand-dependent signalling, induced by binding of ephrin-A1 to EPHA2, causes receptor

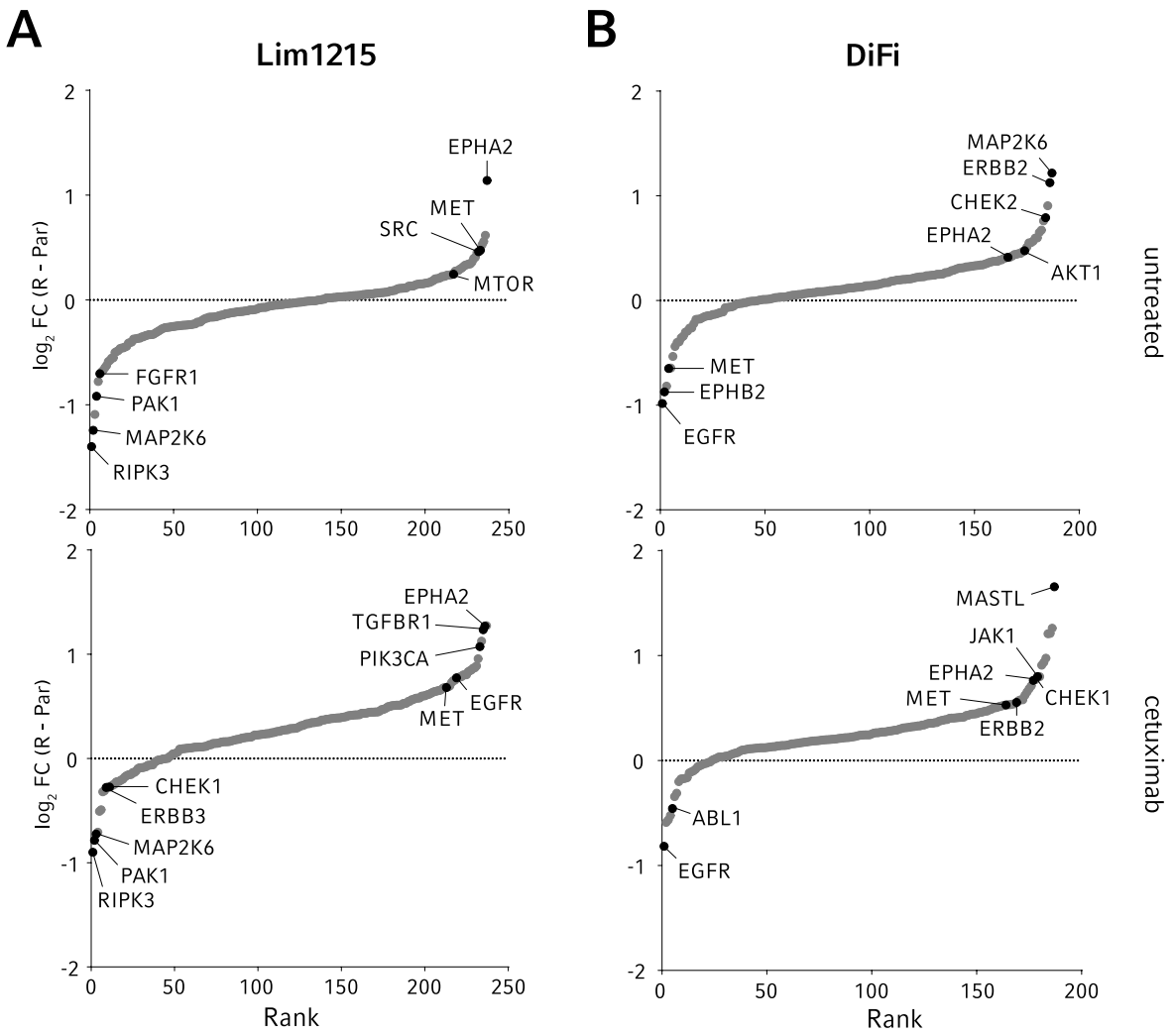

Figure 4.9: EPHA2 is consistently overexpressed in all resistant Lim1215 and DiFi cell lines. **(A, B)** Rank plot of kinases by log_2 fold change (FC) expression in resistant (R) compared to parental (Par) cells from lowest to highest shows EPHA2 as common overexpressed kinase in Lim1215-R **(A)** and DiFi-R **(B)**.

homo-oligomerisation, tyrosine autophosphorylation and downstream signalling, which inhibits cell proliferation, cell adhesion and cell migration (Fig. 4.10B) (Kania & Klein, 2016; Miao et al., 2000, 2009). Ligand-independent EPHA2 signalling however, which is active in the ligand-free state and is inhibited by ephrin-binding, induces cell migration and adhesion (Miao et al., 2009). In cancer, EPHA2 has been ascribed both oncogenic and tumour suppressive qualities. Since the elucidation of the EPHA2-receptor signalling dichotomy it is generally accepted that EPHA2 serves as an oncogene through its ligand-independent signalling, linking it to neoangiogenesis, cell proliferation and cell migration in various malignant entities, including glioma, prostate cancer, NSCLC, breast cancer and CRC (Dunne et al., 2016; Martini et al., 2019; Miao et al., 2009).

Previous findings have linked oncogenic RAS signalling in CRC to EPHA2 overexpression (Dunne et al., 2016). In the proteomic dataset, CET treated Lim1215-R and DiFi-R respectively displayed 2,4- (p=0,0095) and 1,7-times (p=0,0273)

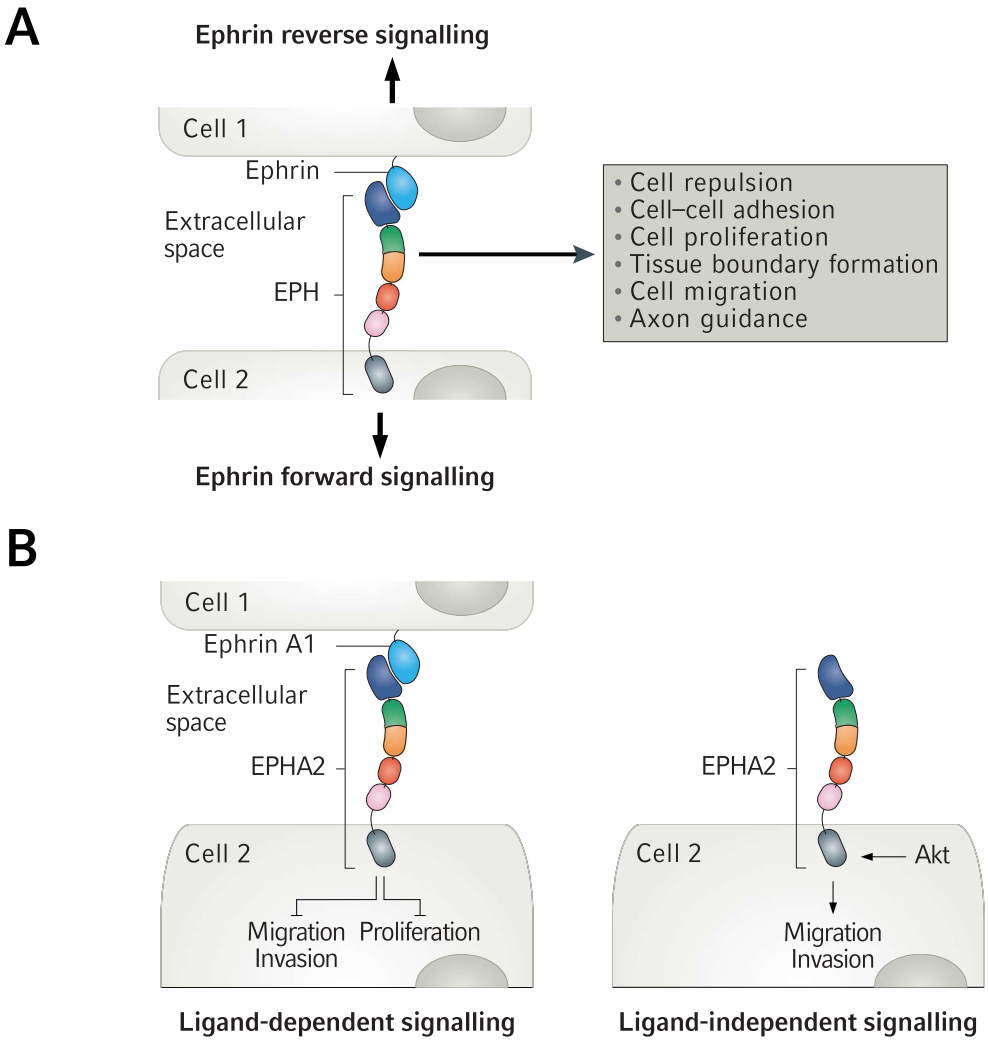

Figure 4.10: (A) EPH tyrosine kinase receptors and their ligands ephrins are involved in short-distance signalling between cells. **(B)** EPHA2 ligand-dependent signalling by binding of Ephrin A1 inhibits cell proliferation and cell migration. In the ligand-independent state, EPHA2 serves as a substrate for Akt and mediates cell migration and invasion.
Adapted from Kania & Klein, 2016.

stronger EPHA2-overexpression than in treated parental cell lines. This was confirmed by Western blotting (Fig 4.11), where EPHA2 expression was on average 4,3- (Lim1215-R1), 5,0- (Lim1215-R2), 3,4- (DiFi-R1) and 11,6- (DiFi-R2) times higher than in parental cells (p<0,05 in all resistant cell lines). Interestingly, EPHA2 overexpression was independent of CET treatment. These results concur with previous findings that identify EPHA2 overexpression as a downstream effect of oncogenic RAS signalling in CRC (Cuyàs et al., 2017; Dunne et al., 2016).

This proteomic dataset reveals widespread kinome reprogramming in CET resistant cell lines. EPHA2 being the only commonly overexpressed kinase in all resistant cell lines suggests it may be a mediator of *KRAS* associated, acquired CET resistance. EPHA2 overexpression in resistant cells, which seems to be independent of CET

treatment, may serve as a novel target for second-lines treatment in resistant CRC cell lines.

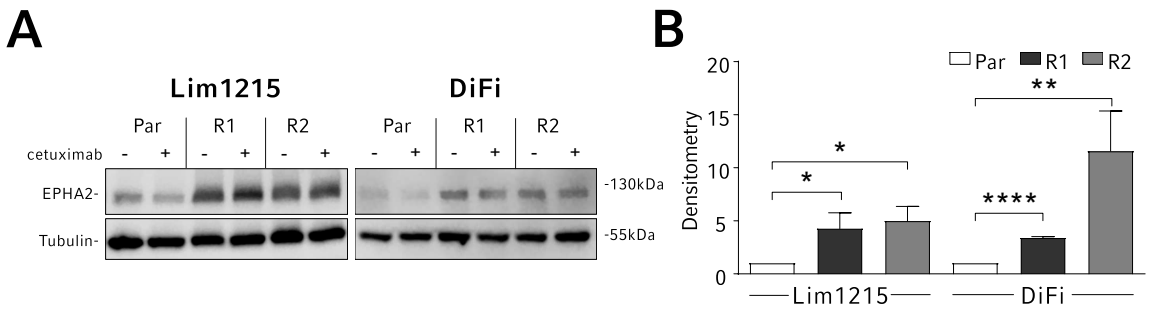

Figure 4.11: EPHA2 overexpression is independent of CET treatment. **(A)** Western blot of parental cells (Par) and CET resistant cells (R1 & R2) confirm EPHA2 overexpression in resistant cells independantly of CET treatment. **(B)** Densitometric data representative of 3 Western blots shows EPHA2 overexpression in untreated resistant cell lines (data represent mean ± SEM). Student's *t* test, $p<0,05$ in all samples.

4.5 EPHA2 IS A TARGETABLE DRIVER OF MIGRATION IN CET RESISTANT CRC CELL LINES

In this mass-spectrometric approach, EPHA2 is the only kinase overexpressed in all four resistant cell lines. Previous findings link EPHA2 overexpression in CRC with increased migration and aggressiveness (Dunne et al., 2016). EPHA2 signalling is both tumour-suppressive and oncogenic, depending on ligand and receptor expression. Active EPHA2 kinase signalling (i.e. ligand-dependent signalling), induced by binding of its ligand ephrin-A1, is characterised by tyrosine autophosphorylation (Y772 amongst others) and downstream tumour-suppressive signalling, which inhibits migration and MAPK signalling (Cuyàs et al., 2017; Dunne et al., 2016; Miao et al., 2000, 2001). In absence of its ligand however, EPHA2 is phosphorylated by AKT1 at S897, establishing ligand-independent signalling, which has been known to drive oncogenic signalling and migration (Miao et al., 2009). Ephrin-A1 was not identified in the mass-spectrometric dataset. However, both *EPHA2* and *EFNA1* (ephrin A1 gene) were transcriptionally expressed in all cell lines as shown by Johanna Albert, M.Sc., by reverse transcription quantitative real-time PCR (RT-qPCR) (Albert, 2019). Gene expression data showed *EPHA2* overexpression in resistant cell lines, while *EFNA1* expression remained at parental baseline levels, illustrating ligand-receptor imbalance in CET resistant cell lines (Fig. 4.12A, $p<0,01$ for all resistant cell lines). Lim1215-R and DiFi-R cell lines also displayed increased S897 EPHA2 phosphorylation compared to their parental counterparts, indicating increased ligand-independent, oncogenic signalling (Fig. 4.12B). Importantly, Y772 EPHA2 phosphorylation remained relatively similar to parental cell lines (Fig. 4.12B). Taken together, this is strongly indicative of active ligand-independent signalling in CET resistant cell lines, which would drive migration and oncogenic signalling in these cells. Indeed, when tested for migration using Transwell® membranes resistant

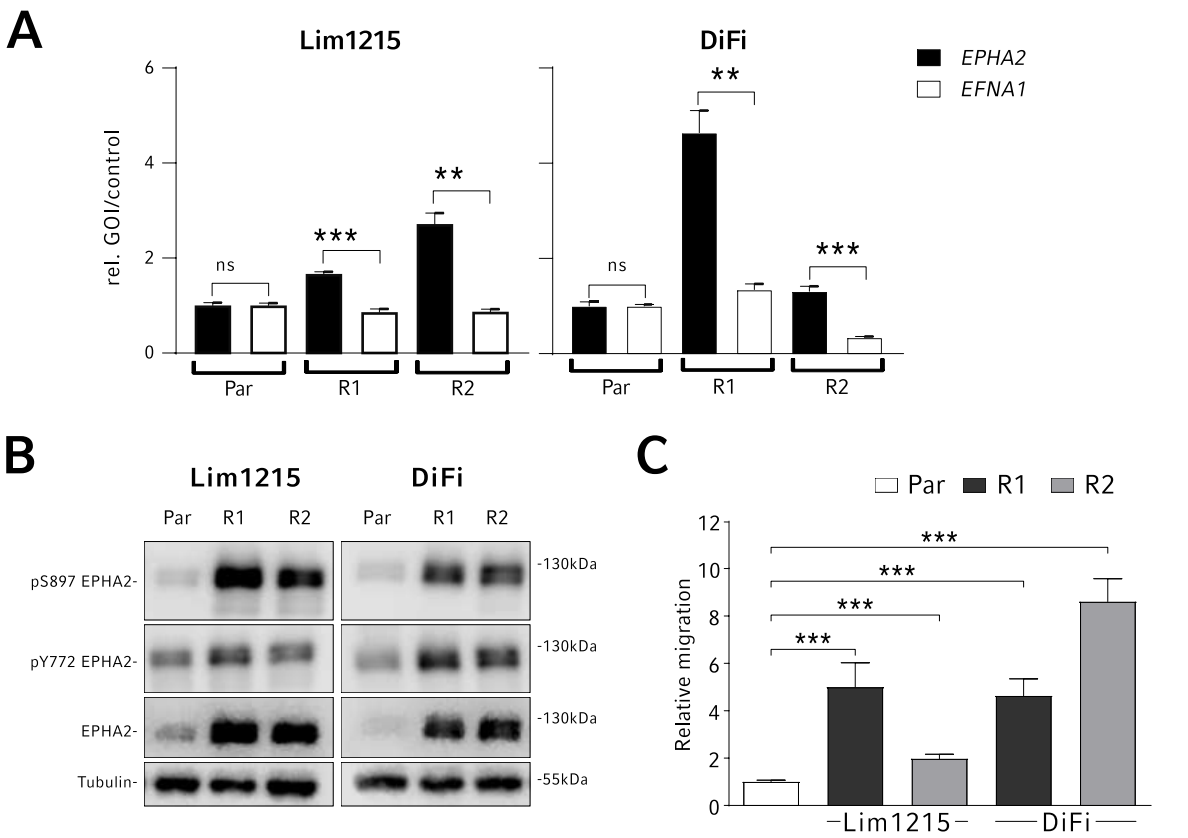

Figure 4.12: EPHA2 ligand-independent signalling may explain increased migration rates in Lim1215-R and DiFi-R cell lines. **(A)** RT-qPCR show *EPHA2* gene overexpression in resistant cell lines (R1 & R2) while EFNA1 expression remains at parental (Par) baseline level in Lim1215 and DiFi cell lines (representative of three biological replicates; data represent mean ± SD of three technical replicates; Student's *t* test, $p<0,01$ in all resistant cell lines). **(B)** Western blots show increased pS897 EPHA2 phosphorylation in resistant compared to parental cell lines, while pY772 EPHA2 phosphorylation stays relatively low, indicative of ligand-independent signalling in Lim1215-R and DiFi-R cell lines. **(C)** Transwell® assays show migration was significantly higher in all resistant cell lines than in parental cell lines (Par) (mean ± SEM of four biological replicates; Student's *t* test, $p<0,001$ in all resistant cell lines).
(A & B) Adapted from data generated by Johanna Albert (Albert, 2019).

cells displayed a significantly higher migration rate, migrating 5,0- (Lim1215-R1), 2,0- (Lim1215-R2), 4,6- (DiFi-R1) and 8,6- (DiFi-R2) times more than their parental counterpart (Fig. 4.12C, $p<0,001$ for all resistant cell lines).

In order to investigate whether EPHA2 is a molecular driver of migration in Lim1215-R and DiFi-R cell lines, EPHA2 signalling was targeted using dasatinib, a well-known but rather unspecific EPHA2 small molecule inhibitor, which is approved for treatment of BCR-ABL fusion gene (*BCR-ABL)* positive chronic myeloid leukaemia (CML) (FDA application no. 021986 & 022072). At 300nM, a concentration that did not affect cell viability (Fig. 4.13A-B), dasatinib could significantly reduce cell

migration in resistant cell lines by 50-90% (Fig 4.13C, p<0,01 compared to vehicle control treatment).

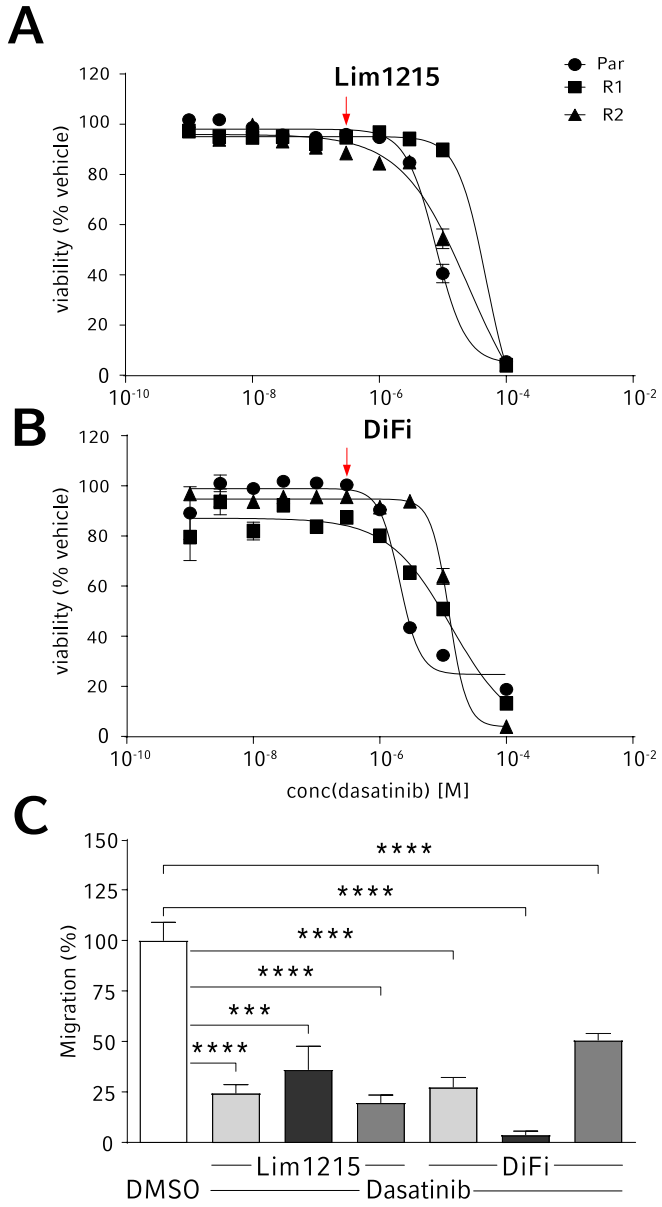

Figure 4.13: Unspecific EPHA2 targeting successfully inhibits migration in Lim1215-R and DiFi-R. **(A, B)** Lim1215 and DiFi, parental (Par) and resistant cell lines (R1 & R2) were treated for 72h with increasing doses of dasatinib. Viability was measured using alamarBlue® (respectively representative of 3 experiments; mean relative viability ± SEM compared to vehicle control of 3 technical replicates).
(C) Dasatinib treatment at 300nM (**A** & **B**, red arrow) significantly decreased migration in resistant cell lines (representative of 3 biological replicates; mean ± SEM of 3 technical replicates; Student's *t* test; p<0,01 in all experiments compared to parental cell lines).

As dasatinib has many other targets beside EPHA2 (off-target effects), a more specific approach was selected to test whether EPHA2 was indeed a molecular driver of migration. Johanna Albert showed that silencing *EPHA2* gene expression using RNA interference (RNAi) was highly successful and reduced migration by more than 80% in all Lim1215-R and DiFi-R cell lines (Fig 4.14, p<0,001 compared to scrambled siRNA control) (Albert, 2019).

Specific targeting of the EPHA2-signalling axis was also achieved by stimulating resistant cells using recombinant ephrin-A1 (ephrin-A1-Fc), which induces ligand-dependent EPHA2 signalling, thus reducing EPHA2 mediated migration and adhesion and causing receptor internalisation and degradation (Miao et al., 2000). Ephrin-A1-Fc treatment successfully depleted EPHA2 levels as shown by Western blot (Fig.

4.15A) and reduced migration by 60-90% in all resistant cell lines (Fig 4.15B, p<0,001 compared to Fc-control treatment).

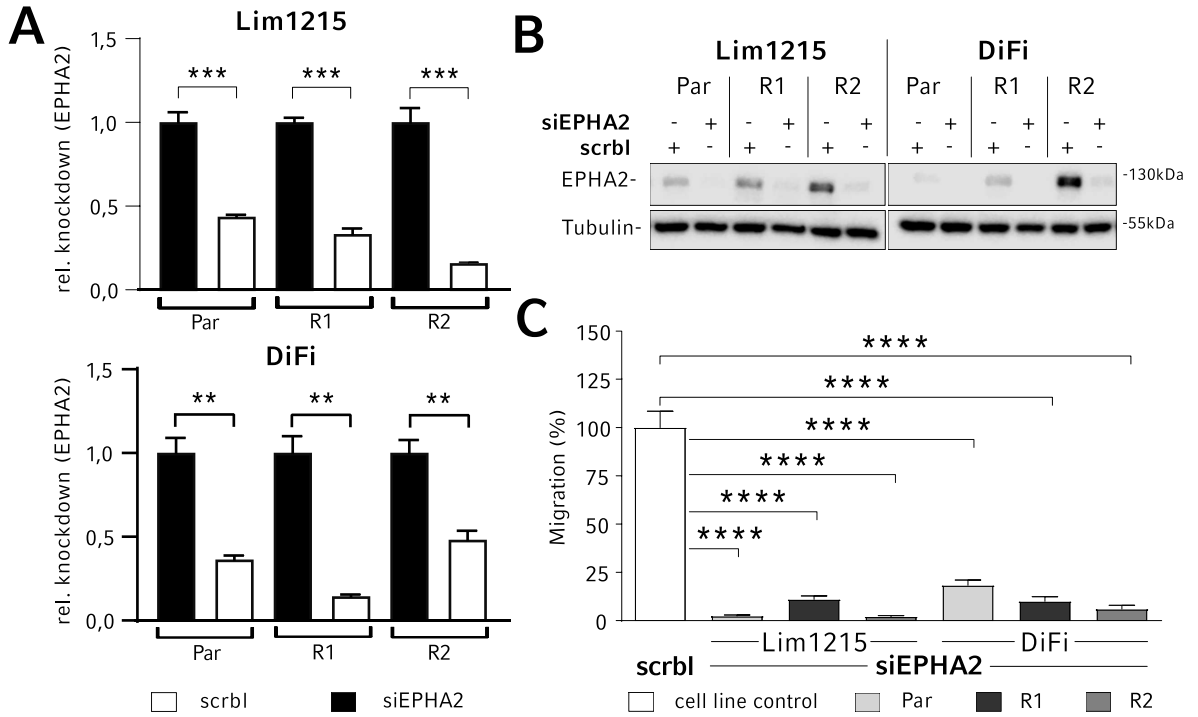

Figure 4.14: EPHA2 is a specific driver of migration in Lim1215-R and DiFi-R. **(A)** RT-qPCR show successful *EPHA2* knockdown using RNAi in all Lim1215 and DiFi cell lines (representative of 3 experiments; mean relative change to parental cell lines ± SEM of technical triplicates; two-sided Student's *t* test, $p < 0,01$ for all cell lines). **(B)** Western blots show EPHA2 depletion 24h after RNAi. **(C)** Migration rates in Lim1215-R and DiFi-R cell lines were significantly decreased by *EPHA2* gene knockdown using RNAi (representative experiments of 3 biological replicates; mean ± SEM of 3 technical replicates; Student's *t* test, p<0,001 compared to cell line control). scrbl: scrambled siRNA control.
Adapted from data generated by Johanna Albert (Albert, 2019).

In an attempt to find a more specific pharmaceutical treatment option than dasatinib, EPHA2-signalling was targeted using anti-EPHA2 (α-EPHA2) antibody treatment. Anti-EPHA2 antibody treatment has shown promising results in the treatment of melanoma, breast cancer and gastric cancer (Hasegawa et al., 2016; Sakamoto et al., 2018). Antibody treatment using a commercially available polyclonal α-EPHA2 Western blotting antibody that binds to the extracellular domain of EPHA2 successfully depleted EPHA2 (Fig. 4.15C) and significantly reduced migration rates by 20-50% in all resistant cell lines (Fig 4.15D, p<0,001 compared to α-GFP, green fluorescent protein, antibody control).

Interestingly, targeting of the EPHA2-signalling axis with dasatinib at 300nM did not notably restore CET sensitivity in resistant cell lines at CET concentrations that significantly affect parental cell lines (5µg/ml) (Figure 4.16). Unexpectedly a partial sensitivity to both CET and dasatinib was observed in DiFi R1 cells, with a minor

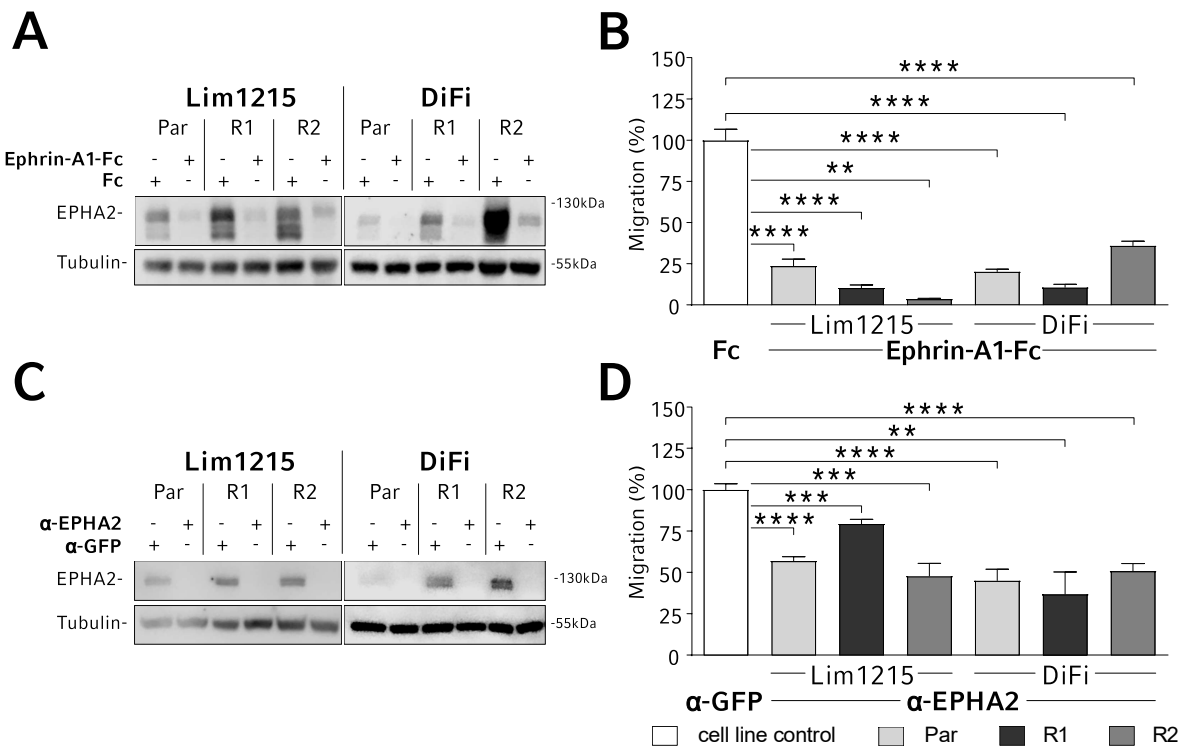

Figure 4.15: Targeting the EPHA2 signalling axis inhibits migration in Lim1215-R and DiFi-R. **(A, C)** Western blots show EPHA2 depletion 24h after ephrin-A1-Fc stimulation **(A)** and anti-EPHA2 antibody treatment **(C)**. **(B, D)** Migration rates were significantly decreased by stimulating EPHA2 using recombinant ephrin-A1-Fc **(B)** and by targeting EPHA2 using anti-EPHA2 antibody treatment **(D)** (representative experiments of 3 biological replicates; mean ± SEM of 3 technical replicates; Student's *t* test, $p<0,01$ in all experiments when compared to cell line control). Fc: IgG1-Fc control. **α**-GFP: anti-GFP antibody. **α**-EPHA2: anti-EPHA2 antibody treatment. **(A)** Western blot generated by Johanna Albert (Albert, 2019).

synergistic effect when combining both drugs. As DiFi R1 had displayed no CET or DASA sensitivity in any of the previous experiments (Fig. 4.1B, Fig. 4.13B) and considering the lack of synergistic effect in all other three resistant cell lines (including isogenic cell line DiFi R2), this was considered an outlier and no further investigations were performed. These results indicate that EPHA2 overexpression and ligand-independent signalling may be an effector of migration but not of proliferation in resistant cells.

Taken together, these results show EPHA2 to be a molecular driver of migration in CET resistant cell lines and a suitable target for a precision-medicine approach.

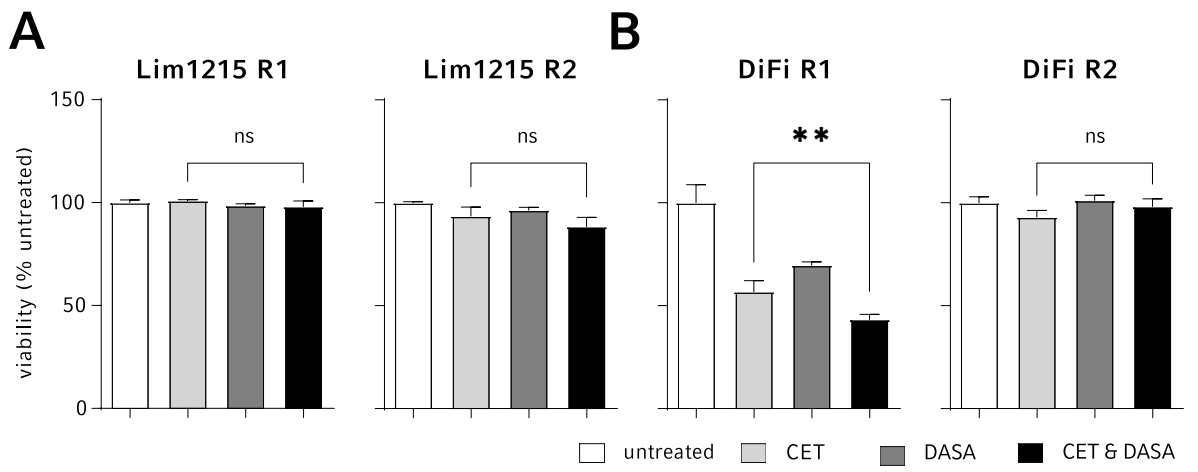

Figure 4.16: Targeting EPHA2 does not restore sensitivity to CET.
(A) Combination treatment of dasatinib (DASA, 300nM) and cetuximab (CET, 5µg/ml) does not notably affect cell viability compared to single-agent treatment in resistant Lim1215 **(A)** and resistant DiFi **(B)** cell lines (mean viability ± SD of technical quadruplicates; two-sided Student's *t* test). ** = $p < 0{,}01$.

4.6 EPHA2 MAY BE OVEREXPRESSED IN MCRC PATIENTS WITH ACQUIRED CET RESISTANCE

In this model of acquired CET resistance EPHA2 overexpression was found to be a molecular driver of migration in resistant cell lines. Previous studies have shown EPHA2 overexpression to be a poor prognostic marker in patients with UICC stage II/III CRC owing to the increased migratory and invasive character of EPHA2 expressing tumours (Dunne et al., 2016). In UICC stage IV mCRC patients, EPHA2 expression correlated with disease progression and worse outcome under FOLFIRI plus CET treatment, indicating EPHA2 play a role in primary treatment resistance (Martini et al., 2019).

In order to translate the findings of this cell line-based study into a clinical setting, the role of EPHA2 expression was investigated in the context of primary CET resistance, metastatic dissemination and acquired CET resistance.

Firstly, EPHA2 was investigated in the context of primary CET resistance. *EPHA2* gene expression was measured using RNA sequencing (RNAseq) in a transcriptomic dataset established during the FIRE-3 trial (Heinemann et al., 2014; Stintzing et al., 2012). The FIRE-3 trial investigated FOLFIRI plus CET versus FOLFIRI plus bevacizumab, an anti-vascular endothelial growth factor A (VEGF-A) antibody, in mCRC. The trial originally recruited patients regardless of their *RAS* status, until *RAS* was found to be linked to primary CET resistance, from which point on an amendment excluded patients with *RAS* mutations from the trial. 211 mCRC patients randomised for FOLFIRI plus CET treatment were recruited before the study amendment and were later classified into *RAS* mutated (*RAS*mt) and *RAS* wildtype (*RAS*wt) (Stintzing et al., 2012). Transcriptomic data from 187 (84%) of these patients (57 *RAS*mt and 130 *RAS*wt), were available for *EPHA2* expression analysis. As previously shown, *RAS*

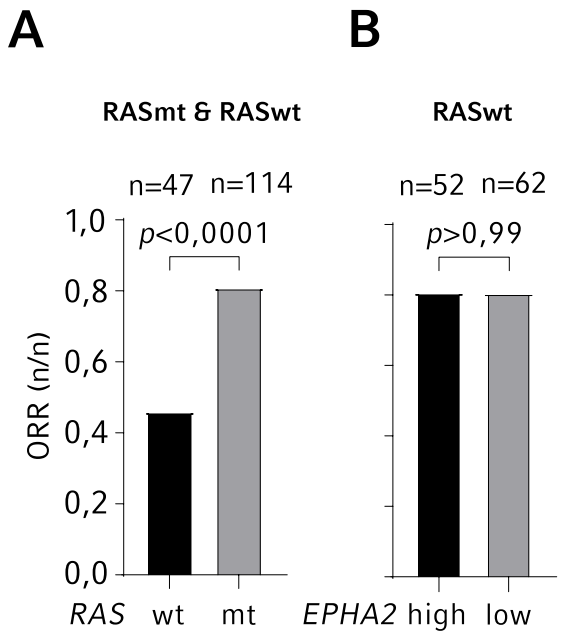

Figure 4.17: EPHA2 is not a biomarker of primary CET resistance in mCRC patients. (**A**) Data from 130 patients with *RAS* wildtype (*RAS*wt) and 57 patients with *RAS* mutated (*RAS*mt) UICC stage IV mCRC treated with CET in the FIRE-3 trial show *RAS*mt status was an excellent predictor of poor therapy response to CET (Fisher's exact test, $p<0,0001$). In *RAS*wt patients, *EPHA2* high and low patients showed no significant difference in (**B**) objective response rate (ORR; responders/n), (**C**) progression free survival (PFS) or (**D**) overal survival (OS) under CET treatment (log-rank test).
(A) Adapted from Stintzing et al., 2012.

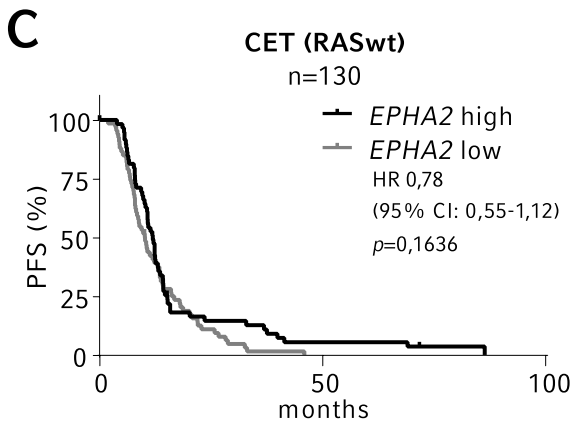

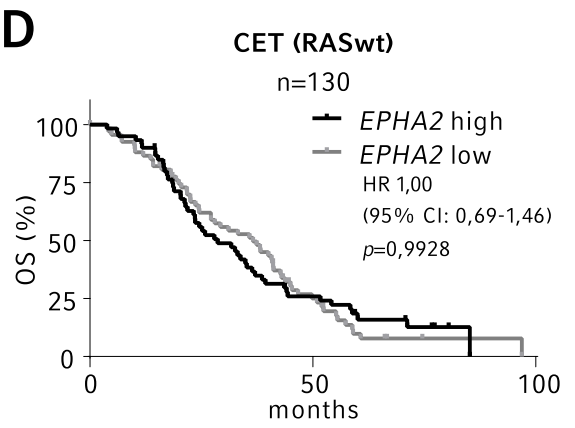

mutational status was an excellent predictor of poor treatment response (ORR, objective response rate – responders to treatment/n) to FOLFIRI plus CET as defined by RECIST-criteria, with *RAS*mt patients responding significantly less to the combination treatment than *RAS*wt patients (Fig. 4.17A, ORR_{RASmt}=0,4468; ORR_{RASwt}=0,8070; Fisher's exact test, $p<0,0001$) (Stintzing et al., 2012). This confirms previous findings linking *RAS*mt status to primary CET resistance, which triggered the FIRE-3 trial amendment (Bokemeyer et al., 2009; Van Cutsem et al., 2009). *RAS*mt patients were excluded and *EPHA2* assessed in *RAS*wt patients alone, separating patients into $EPHA2_{high}$ and $EPHA2_{low}$, as defined by the median *EPHA2* gene expression level. In *RAS*wt patients *EPHA2* expression levels could not be correlated to worst treatment outcome (ORR), indicating it does not play a role in primary resistance against FOLFIRI plus CET treatment (Fig. 4.17B, $ORR_{EPHA2high}$=0,8077; $ORR_{EPHA2low}$=0,8065; Fisher's exact test, p>0,9999). Using the Kaplan-Meyer method, *EPHA2* expression could not be linked to worse outcome in *RAS*wt patients. Neither progression free survival (PFS) nor overall survival (OS) differed between the $EPHA2_{high}$ and $EPHA2_{low}$ groups, dismissing it as a marker of poor prognosis (PFS –

hazard ratio of 0,78; 95% CI: 0,55-1,12 | OS – hazard ratio of 1,00; 95% CI: 0,69-1,46) (Fig. 4.17C-D). These results oppose previous findings (Dunne et al., 2016; Martini et al., 2019) and indicate no link between *EPHA2* expression and primary CET treatment resistance or poor prognosis.

In a next step, in order to assess a possible influence of *EPHA2* on metastatic dissemination, two transcriptomic datasets from the gene expression omnibus (GEO accession GSE40367 & GSE81582) were used to probe *EPHA2* expression levels in paired primary and metastatic CRC tissue (Roessler et al., 2015; Sayagués et al., 2016). In both studies, chemotherapy-naïve mCRC patients underwent radical resection of the primary tumour and synchronous metastases. *EPHA2* gene expression levels from paired primary CRC tumours and synchronous metastases (n=25) showed no *EPHA2* overexpression in metastatic tissue, thereby suggesting it plays no role in metastatic dissemination in chemotherapy naïve patients (Fig. 4.18A).

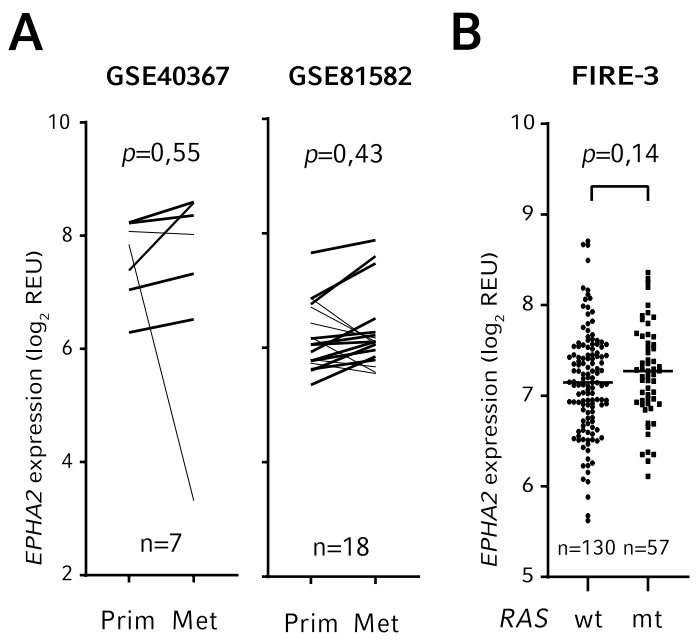

Figure 4.18: EPHA2 is not overexpressed in metastatic tissue or in primary *RAS*mt tumours. **(A)** Published transcriptomic data downloaded from GEO show *EPHA2* was not significantly overexpressed in synchronous CRC metastases compared to their primary tumours (paired Student's *t* test). **(B)** In the FIRE-3 trial *EPHA2* was not significantly overexpressed in *RAS*mt primary tumours compared to *RAS*wt tumours (unpaired Student's *t* test). REU: relative expression units.

In another approach, transcriptomic data from the FIRE-3 trial was probed for a possible link between *RAS* status and *EPHA2* gene expression. *EPHA2* has previously been shown to be overexpressed as a downstream effector of active RAS signalling through activation of the MAPK and Ras-Like signalling (Ral) pathways (Dunne et al., 2016). Consequently, *EPHA2* should be transcriptionally overexpressed in *RAS*mt CRC, where *RAS* mutations should induce constitutively active *RAS* signalling. When comparing *EPHA2* in both *RAS*mt and *RAS*wt subsets of mCRC patients within the FIRE-3 trial, a slight *EPHA2* overexpression was detectable in the *RAS*mt group, though this did not reach significance (median expression: $EPHA2_{RASwt}$=7,14 REU; $EPHA2_{RASmt}$=7,27 REU, p=0.1415) (Fig. 4.18B). These results indicate *EPHA2* was not overexpressed in primary *RAS*mt tumours.

Finally, in order to translate the experimental findings from this cell line-based model of acquired CET resistance in a clinical setting, a transcriptomic dataset from mCRC patients with acquired CET resistance was used to assess EPHA2 in the context of acquired *KRAS* mediated CET resistance. Unfortunately, there are only very few studies available in which paired tissue from before treatment with anti-EGFR targeted therapies and from after gain of resistance is available. The Prospect-C trial recruited 46 mCRC patients that underwent tissue biopsy both before single-agent CET treatment and after disease progression as defined by RECIST-criteria (Woolston et al., 2019). Patients were classified according to the response to single-agent CET treatment into patients with primary progression (i.e. primary CET resistance) and with prolonged benefit: primary disease progression was defined as disease progression before or at the first computed tomography scan (at 12 weeks), all other

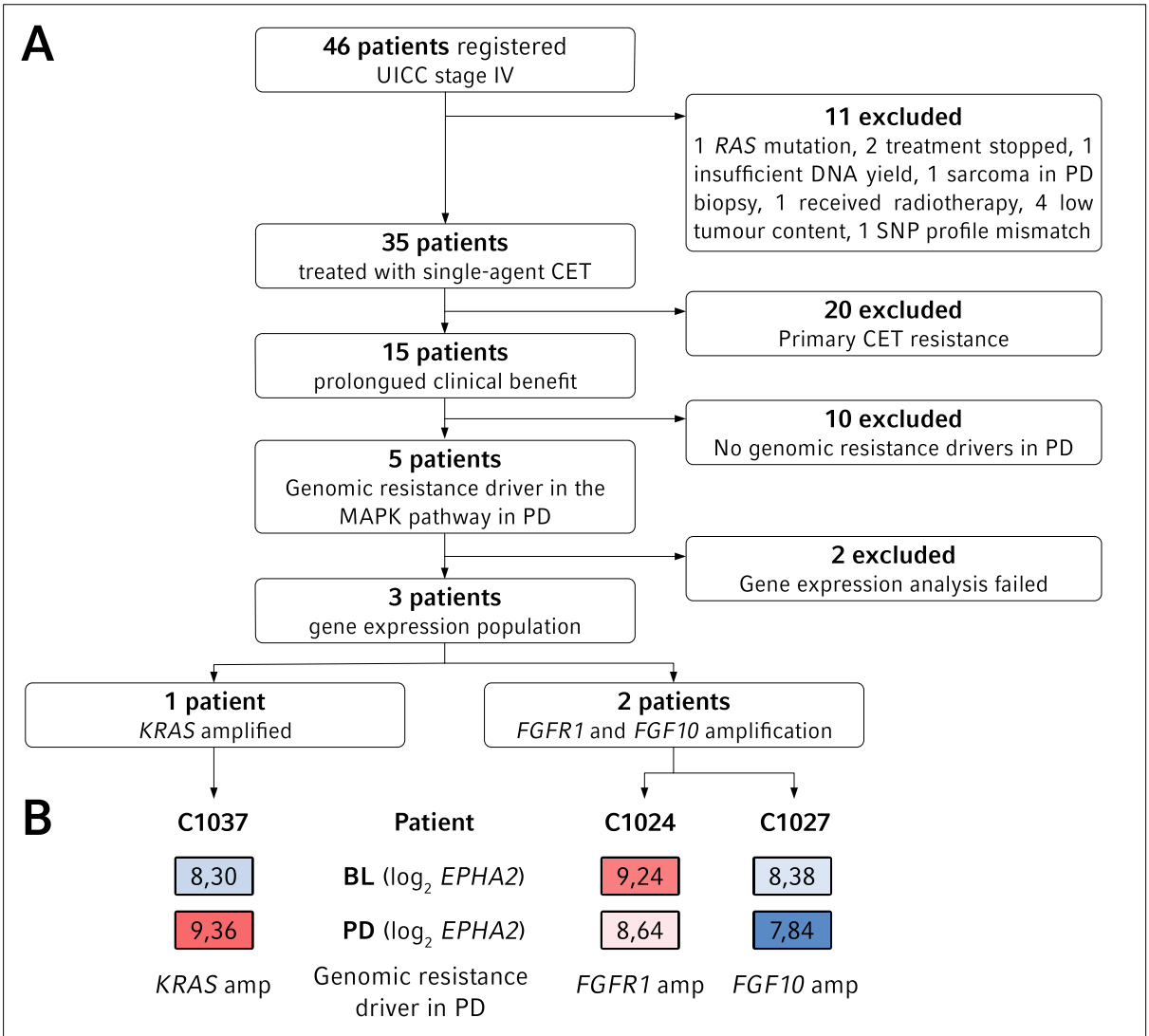

Figure 4.19: *EPHA2* may be overexpressed in CET resistant, *KRAS* altered mCRC patients. **(A)** Prospect-C trial CONSORT diagram. **(B)** Tumour transcriptomic and genomic characteristics (*EPHA2* expression level in relative expression units). BL: baseline biopsy. PD: progressive disease biopsy. SNP: single nucleotide polymorphism. amp: gene amplification.

patients were considered to show prolonged benefit. Baseline (BL) and progressive disease (PD) biopsies were subjected to genomic and transcriptomic analysis in order to identify genomic and non-genomic resistance drivers. The Prospect-C trial included data from 15 patients that showed prolonged clinical benefit from single-agent CET treatment before developing progressive disease (PD) (i.e. secondary CET resistance) (Fig. 4.19A). Acquired genomic resistance drivers in the MAPK pathway were identified in 5 of these 15 patients (33%) (patients C1005, C1024, C1025, C1027 & C1037), 3 of which displayed *KRAS* alterations (activating mutations or amplifications - *KRAS*mt) as a resistance mechanism, mirroring the cell line model of acquired CET resistance used in this study, the other 2 displaying other genomic alterations within the MAPK-pathway. Transcriptomic data were available for only three of these five patients (C1024, *KRAS*wt; C1027 *KRAS*wt; C1037; *KRAS*mt). Comparison of transcriptomic data from the baseline biopsies (BL) and progressive disease biopsies (PD) showed a strong *EPHA2* overexpression in the C1037PD sample (log_2 FC(PD-BL) = 1,06), which had developed a novel *KRAS* amplification in the PD biopsy, while no *KRAS* alteration was identifiable in the baseline biopsy (Fig. 4.19B). Samples C1024PD and C1027PD1 displayed other genomic alterations than *KRAS* (fibroblast growth factor receptor 1, *FGFR1* amplification and fibroblast growth factor 10, *FGF10* amplification respectively) but displayed no *EPHA2* overexpression in the PD compared to the BL tissue (log_2 FC=-0,60 and log_2 FC=-0,54 respectively) (Fig. 4.19B). These results may mirror the cell line model used in this study: acquired CET resistance mediated by secondary *KRAS* alterations (amplification in patient C1037 and in the DiFi-R cell lines) may be associated with *EPHA2* overexpression. Unfortunately, the association between *KRAS*mt status and *EPHA2* overexpression did not reach significance, almost certainly due to the small sample size (Fisher's exact test, p=0,133).

Taken together, these results collide with previous findings linking *EPHA2* to primary CET resistance. These results also refute a link between *EPHA2* and metastatic dissemination but indicate a possible *EPHA2* overexpression in the context of *KRAS* associated, secondary CET resistance, although a prospective study involving a larger cohort undergoing CET treatment is required to confirm this.

5 Discussion

In this model of CET resistance, reprogramming of the proteome and kinome was assessed in *KRAS* altered, CET resistant mCRC cell lines using kinase expression levels and by inferring kinase activity through downstream phosphorylation patterns.

Resistant cell lines displayed significant reprogramming of the proteome and kinome, mainly exhibiting individual changes to each resistant cell line. A common feature uncovered in all resistant cell lines was EPHA2 overexpression, which was found in all four independently established resistant cell lines harbouring *KRAS* alterations. EPHA2 overexpression in these cells might be linked to activating *RAS* alterations as RAS signalling was shown to induce EPHA2 overexpression through the MAPK and Ras-Like signalling (Ral) pathways (Cuyàs et al., 2017; Dunne et al., 2016). This might explain consistent EPHA2 overexpression in *KRAS* altered Lim1215-R and DiFi-R cell lines, independently of CET treatment. No common pattern of kinase over-activation (as opposed to overexpression) was found by kinase-substrate motif enrichment. The phosphoproteomic dataset was interpreted with care, owing to the low quantity of data and the lower biological reliability of the dataset. The low quantity and subsequent low reliability of the phosphoproteomic data was most likely due to the low protein quantity used in the LC-MS/MS experiment, as illustrated by the low number of identified phosphosites (n=1497 in Lim1215 cell lines and n=1279 in DiFi cell lines). The limited biological reliability was supported by the missing signs of EPHA2 oncogenic signalling in the phosphoproteomic data, which would have presented through S897 over-phosphorylation of EPHA2 and phosphorylation of downstream EPHA2 substrates, such as focal adhesion kinase 1 (FAK1). Neither EPHA2 nor many of its substrates were identified in the phosphoproteomic fraction, thereby explaining the missing signs of overactive EPHA2-signalling in the subsequent analyses. A higher protein quantity would have yielded more data and a more reliable dataset. The difficult analysis of kinase activity raises the question of potential kinases other than EPHA2 that may be involved in CET resistance and may have been missed. However successful functional targeting of EPHA2 highlights the importance of the role that EPHA2 signalling plays in the phenotype of resistant cells.

EPHA2 was found to be overexpressed in all CET resistant cell lines. As described earlier, EPHA2 has been ascribed both pro- and anti-tumourigenic effects in cancer. Ligand-dependent signalling, driven by EPHA2 tyrosine autophosphorylation after ephrin-A1 binding, causes FAK1 dephosphorylation and thereby negatively regulates cell adhesion and migration (Miao et al., 2000). In its ligand-independent state, EPHA2 is phosphorylated by AKT1 at serine 897 (S897), which drives cell migration and invasion (Miao et al., 2009). Importantly, ephrin-A1 stimulation of EPHA2 causes pS897 dephosphorylation. In Lim1215-R and DiFi-R, *EPHA2* was overexpressed while *EFNA1* remained at baseline level, suggesting ligand-receptor imbalance in these cells. Coupled with the increased EPHA2 phosphorylation at S897 in Lim1215-R and DiFi-R cell lines, these results indicate active ligand-independent signalling in these CET resistant cell lines. As expected, resistant cells migrated significantly more than their parental counterparts. This increased migration in resistant cells could be

successfully inhibited by targeting EPHA2 signalling using dasatinib or by rectifying EPHA2 receptor-ligand imbalance through depletion of EPHA2 using RNAi or antibody treatment, as well as by stimulation with recombinant ephrin-A1. Intriguingly, parental cells were also affected by the treatment. This suggests that EPHA2 signalling may also be active in these cells, albeit with significantly lower intensity, as shown by their low basal migration rate.

Targeting EPHA2 did not restore CET sensitivity in resistant cells, indicating it does not play a role as a resistance driver of cellular proliferation, as was observed in a model of primary *KRAS* associated CET resistance (Martini et al., 2019). It is more likely that EPHA2 serves as a downstream driver of migration in *KRAS* associated CET resistance.

The results of the functional experiments described above, underpinned by previous findings, support the use of EPHA2 targeted therapies in CET resistant mCRC. An anti-EPHA2 therapeutic approach may help to inhibit cell migration, and may contribute to reducing metastatic dissemination. Cell metastasis being a more multi-faceted process than migration alone, this hypothesis would have to be validated in *vitro* invasion assays and in *vivo* experiments.

In cancer, EPHA2 is one of the most predominant members of the Ephrin receptor family. Its overexpression in several cancer entities including CRC has been linked to treatment resistance and disease progression (Koch et al., 2015; Martini et al., 2019; Miao et al., 2009; Zhuang et al., 2010). In CRC, EPHA2 was found to be a poor prognostic marker in UICC stage II/III disease due to its ability to promote migration and invasion (Dunne et al., 2016). In mCRC patients treated with FOLFIRI plus CET, EPHA2 overexpression correlated to disease progression and worse outcome, identifying it as a biomarker of primary treatment resistance in these patients (Martini et al., 2019). Unlike published data, the transcriptomic dataset from 187 UICC stage IV mCRC patients recruited during the FIRE-3 trial did not support a role for EPHA2 as a biomarker of primary treatment resistance. Alternatively, it is generally possible that transcriptomic data do not reflect EPHA2 protein levels (as measured by Martini *et al.*), owing to the potential difference between gene expression and protein expression levels. Regarding its role in acquired CET resistance, data from the Prospect-C trail showed *EPHA2* gene overexpression in one patient with a secondary *KRAS* amplification. This overexpression was not however found in other patients with other genomic resistance drivers within the MAPK pathway. The tissue of the PD biopsy of patient C1037 in the Prospect-C trial might therefore mirror the cell line model used here, having developed secondary CET resistance through *KRAS* amplification and displaying *EPHA2* overexpression, as seen in the DiFi-R cell lines.

In conclusion, this research project presents evidence that the EPHA2 signalling pathway is activated by kinase overexpression in both *KRAS* altered CET resistant cell lines and in mCRC patients with acquired CET resistance. Functional cell culture experiments and previous studies support the rationale of second-line EPHA2 targeted therapies in acquired CET resistance. Indisputably, this hypothesis remains to be validated in *vivo* experiments and in larger patient cohorts.

6 Bibliography

Albert, J. (2019). *Role of the receptor tyrosine kinase EPHA2 in resistance to the anti-EGFR drug cetuximab in colorectal cancer cell lines*. Ludwig-Maximilians-Universität München.

Barrett, T., Wilhite, S. E., Ledoux, P., Evangelista, C., Kim, I. F., Tomashevsky, M., Marshall, K. A., Phillippy, K. H., Sherman, P. M., Holko, M., Yefanov, A., Lee, H., Zhang, N., Robertson, C. L., Serova, N., Davis, S., & Soboleva, A. (2013). NCBI GEO: Archive for functional genomics data sets - Update. *Nucleic Acids Research*, *41*(D1), 991–995. https://doi.org/10.1093/nar/gks1193

Blume-Jensen, P., & Hunter, T. (2001). Oncogenic kinase signalling. *Nature*, *411*(6835), 355. https://doi.org/10.1038/35077225

Bokemeyer, C., Bondarenko, I., Makhson, A., Hartmann, J. T., Aparicio, J., De Braud, F., Donea, S., Ludwig, H., Schuch, G., Stroh, C., Loos, A. H., Zubel, A., & Koralewski, P. (2009). Fluorouracil, leucovorin, and oxaliplatin with and without cetuximab in the first-line treatment of metastatic colorectal cancer. *Journal of Clinical Oncology*, *27*(5), 663–671. https://doi.org/10.1200/JCO.2008.20.8397

Boyden, S. (1962). The chemotactic effect of mixtures of antibody and antigen on polymorphonuclear leucocytes. *Journal of Experimental Medicine*, *115*(3), 453–466. https://doi.org/10.1084/jem.115.3.453

Bradford, M. M. (1976). A Rapid and Sensitive Method for the Quantitation of Microgram Quantities of Protein Utilizing the Principle of Protein-Dye Binding. *Analytical Biochemistry*, *72*, 248–254. https://doi.org/10.1016/j.cj.2017.04.003

Candeil, L., Gourdier, I., Peyron, D., Vezzio, N., Copois, V., Bibeau, F., Orsetti, B., Scheffer, G. L., Ychou, M., Khan, Q. A., Pommier, Y., Pau, B., Martineau, P., & Del Rio, M. (2004). ABCG2 overexpression in colon cancer cells resistant to SN38 and in irinotecan-treated metastases. *International Journal of Cancer*, *109*(6), 848–854. https://doi.org/10.1002/ijc.20032

Cuyàs, E., Queralt, B., Martin-castillo, B., Bosch-barrera, J., & Menendez, J. A. (2017). EphA2 receptor activation with ephrin-A1 ligand restores cetuximab efficacy in NRAS -mutant colorectal cancer cells. *Oncology Reports*, 263–270. https://doi.org/10.3892/or.2017.5682

De Mattia, E., Cecchin, E., & Toffoli, G. (2015). Pharmacogenomics of intrinsic and acquired pharmacoresistance in colorectal cancer: Toward targeted personalized therapy. *Drug Resistance Updates*, *20*, 39–70. https://doi.org/10.1016/j.drup.2015.05.003

Diaz, L. A. J., Williams, R., Wu, J., Kinde, I., Hecht, J. R., Berlin, J., Allen, B., Bozic, I., Reiter, J. G., Nowak, M. A., Kinzler, K. W., Oliner, K. S., & Vogelstein, B. (2012). The molecular evolution of acquired resistance to targeted EGFR blockade in colorectal cancers. *Nature*, *486*(7404), 537–540. https://doi.org/10.1038/nature11219

Dirks, W. G., & Drexler, H. G. (2013). STR DNA Typing of Human Cell Lines: Detection of Intra- And Interspecies Cross-Contamination. *Methods Molecular Biology*, *946*, 27–38. https://doi.org/10.1007/978-1-62703-128-8_3.

Dunne, P. D., Dasgupta, S., Blayney, J. K., Mcart, D. G., Redmond, K. L., Weir, J., Bradley, C. A., Sasazuki, T., Shirasawa, S., Wang, T., Srivastava, S., Ong, C. W., Arthur, K., Salto-tellez, M., Wilson, R. H., Johnston, P. G., & Schaeybroeck, S. Van. (2016). EphA2 Expression Is a Key Driver of Migration and Invasion and a Poor Prognostic Marker in Colorectal Cancer. *Clinical Cancer Research*, *22*(1), 230–243. https://doi.org/10.1158/1078-0432.CCR-15-0603

Eisenhauer, E. A., Therasse, P., Bogaerts, J., Schwartz, L. H., Sargent, D., Ford, R.,

Dancey, J., Arbuck, S., Gwyther, S., Mooney, M., Rubinstein, L., Shankar, L., Dodd, L., Kaplan, R., Lacombe, D., & Verweij, J. (2009). New response evaluation criteria in solid tumours: Revised RECIST guideline (version 1.1). *European Journal of Cancer*, *45*(2), 228–247. https://doi.org/10.1016/j.ejca.2008.10.026

Fabbro, D., Cowan-Jacob, S. W., & Moebitz, H. (2015). Ten things you should know about protein kinases: IUPHAR Review 14. *British Journal of Pharmacology*, *172*(11), 2675–2700. https://doi.org/10.1111/bph.13096

Fearon, E. R., & Vogelstein, B. (1990). A genetic model for colorectal tumorigenesis. *Cell*, *61*(5), 759–767. https://doi.org/10.1016/0092-8674(90)90186-I

Fleuren, E. D. G., Zhang, L., Wu, J., & Daly, R. J. (2016). The kinome "at large" in cancer. *Nature Reviews Cancer*, *16*(2), 83–98. https://doi.org/10.1038/nrc.2015.18

Gnoni, A., Russo, A., Silvestris, N., Maiello, E., Vacca, A., Marech, I., Numico, G., Paradiso, A., Lorusso, V., & Azzariti, A. (2011). Pharmacokinetic and Metabolism Determinants of Fluoropyrimidines and Oxaliplatin Activity in Treatment of Colorectal Patients. *Current Drug Metabolism*, *12*(10), 918–931. https://doi.org/10.2174/138920011798062300

Hanahan, D., & Weinberg, R. A. (2011). Hallmarks of cancer: The next generation. *Cell*, *144*(5), 646–674. https://doi.org/10.1016/j.cell.2011.02.013

Hasegawa, J., Sue, M., Yamato, M., Ichikawa, J., Ishida, S., Shibutani, T., Kitamura, M., Wada, T., & Agatsuma, T. (2016). Novel anti-EPHA2 antibody, DS-8895a for cancer treatment. *Cancer Biology and Therapy*, *17*(11), 1158–1167. https://doi.org/10.1080/15384047.2016.1235663

Heinemann, V., Rivera, F., O'Neil, B. H., Stintzing, S., Koukakis, R., Terwey, J. H., & Douillard, J. Y. (2016). A study-level meta-analysis of efficacy data from head-to-head first-line trials of epidermal growth factor receptor inhibitors versus bevacizumab in patients with RAS wild-type metastatic colorectal cancer. *European Journal of Cancer*, *67*, 11–20. https://doi.org/10.1016/j.ejca.2016.07.019

Heinemann, V., Weikersthal, L. F. Von, Decker, T., Kiani, A., Vehling-kaiser, U., Scholz, M., Müller, S., Link, H., Niederle, N., Rost, A., Höffk, H., Moehler, M., Lindig, R. U., Modest, D. P., Rossius, L., Kirchner, T., Jung, A., Stintzing, S., & Jena, U. (2014). FOLFIRI plus cetuximab versus FOLFIRI plus bevacizumab as first-line treatment for patients with metastatic colorectal cancer (FIRE-3): A randomised, open-label, phase 3 trial. *The Lancet Oncology*, *15*(10), 1065–1075. https://doi.org/10.1016/S1470-2045(14)70330-4

Hornbeck, P. V., Zhang, B., Murray, B., Kornhauser, J. M., Latham, V., & Skrzypek, E. (2015). PhosphoSitePlus, 2014: Mutations, PTMs and recalibrations. *Nucleic Acids Research*, *43*(D1), D512–D520. https://doi.org/10.1093/nar/gku1267

Jollife, I. T., & Cadima, J. (2016). Principal component analysis: A review and recent developments. *Philosophical Transactions of the Royal Society A: Mathematical, Physical and Engineering Sciences*, *374*(2065). https://doi.org/10.1098/rsta.2015.0202

Kanehisa, M., & Goto, S. (2000). KEGG: Kyoto Encyclopedia of Genes and Genomes. *Nucleic Acids Research*, *28*(1), 27–30. https://doi.org/10.3892/ol.2020.11439

Kania, A., & Klein, R. (2016). Mechanisms of ephrin-Eph signalling in development, physiology and disease. *Nature Reviews Molecular Cell Biology*, *17*(4), 240–256. https://doi.org/10.1038/nrm.2015.16

Karapetis, C. S., Khambata-Ford, S., Jonker, D. J., O'Callaghan, C. J., Tu, D., Tebbutt, N. C., Simes, R. J., Chalchal, H., Shapiro, J. D., Robitaille, S., Price, T.

J., Shepherd, L., Au, H.-J., Langer, C., Moore, M. J., & Zalcberg, J. R. (2008). K-ras Mutations and Benefit from Cetuximab in Advanced Colorectal Cancer. *New England Journal of Medicine*, *359*, 1757–1765. https://doi.org/10.1056/NEJMoa1109071

Koch, H., Busto, M. E. D. C., Kramer, K., Médard, G., & Kuster, B. (2015). Chemical proteomics uncovers EPHA2 as a mechanism of acquired resistance to small molecule EGFR kinase inhibition. *Journal of Proteome Research*, *14*(6), 2617–2625. https://doi.org/10.1021/acs.jproteome.5b00161

Leitlinienprogramm Onkologie. (2019). *S3-Leitlinie Kolorektales Karzinom*. (Deutsche Krebsgesellschaft, Deutsche Krebshilfe, AWMF), AWMF Registrierungsnummer: 021/007OL.

Lu, Y., Zhao, X., Liu, Q., Li, C., Graves-Deal, R., Cao, Z., Singh, B., Franklin, J. L., Wang, J., Hu, H., Wei, T., Yang, M., Yeatman, T. J., Lee, E., Saito-Diaz, K., Hinger, S., Patton, J. G., Chung, C. H., Emmrich, S., … Coffey, R. J. (2017). lncRNA MIR100HG-derived miR-100 and miR-125b mediate cetuximab resistance via Wnt/ -catenin signaling. *Nature Medicine*, *December 2016*. https://doi.org/10.1038/nm.4424

Manning, G., Whyte, D. B., Martinez, R., Hunter, T., & Sudarsanam, S. (2002). The protein kinase complement of the human genome. *Science*, *298*(5600), 1912–1934. https://doi.org/10.1126/science.1075762

Manzoni, C., Kia, D. A., Vandrovcova, J., Hardy, J., Wood, N. W., Lewis, P. A., & Ferrari, R. (2018). Genome, transcriptome and proteome: The rise of omics data and their integration in biomedical sciences. *Briefings in Bioinformatics*, *19*(2), 286–302. https://doi.org/10.1093/BIB/BBW114

Martini, G., Cardone, C., Vitiello, P. P., Belli, V., Napolitano, S., Troiani, T., Ciardiello, D., Maria, C., Corte, D., Morgillo, F., Matrone, N., Sforza, V., Papaccio, G., Desiderio, V., Paul, M. C., Moreno-viedma, V., Normanno, N., Rachiglio, A. M., Tirino, V., … Martinelli, E. (2019). EPHA2 Is a Predictive Biomarker of Resistance and a Potential Therapeutic Target for Improving Antiepidermal Growth Factor Receptor Therapy in Colorectal Cancer. *Molecular Cancer Therapeutics*, *18*(4), 845–856. https://doi.org/10.1158/1535-7163.MCT-18-0539

Miao, H., Burnett, E., Kinch, M., Simon, E., & Wang, B. (2000). Activation of EphA2 kinase suppresses integrin function and causes focal-adhesion-kinase dephosphorylation. *Nature Cell Biology*, *2*(2), 62–69. https://doi.org/10.1038/35000008

Miao, H., Li, D. Q., Mukherjee, A., Guo, H., Petty, A., Cutter, J., Basilion, J. P., Sedor, J., Wu, J., Danielpour, D., Sloan, A. E., Cohen, M. L., & Wang, B. (2009). EphA2 Mediates Ligand-Dependent Inhibition and Ligand-Independent Promotion of Cell Migration and Invasion via a Reciprocal Regulatory Loop with Akt. *Cancer Cell*, *16*(1), 9–20. https://doi.org/10.1016/j.ccr.2009.04.009

Miao, H., Wei, B. R., Peehl, D. M., Li, Q., Alexandrou, T., Schelling, J. R., Rhim, J. S., Sedor, J. R., Burnett, E., & Wang, B. (2001). Activation of EphA receptor tyrosine kinase inhibits the Ras/MAPK pathway. *Nature Cell Biology*, *3*(5), 527–530. https://doi.org/10.1038/35074604

Misale, S., Di Nicolantonio, F., Sartore-Bianchi, A., Siena, S., & Bardelli, A. (2014). Resistance to Anti-EGFR therapy in colorectal cancer: From heterogeneity to convergent evolution. *Cancer Discovery*, *4*(11), 1269–1280. https://doi.org/10.1158/2159-8290.CD-14-0462

Misale, S., Yaeger, R., Hobor, S., Scala, E., Janakiraman, M., Liska, D., Valtorta, E., Schiavo, R., Buscarino, M., Siravegna, G., Bencardino, K., Cercek, A., Chen, C.-

T., Veronese, S., Zanon, C., Sartore-Bianchi, A., Gambacorta, M., Gallicchio, M., Vakiani, E., … Bardelli, A. (2012). Emergence of KRAS mutations and acquired resistance to anti-EGFR therapy in colorectal cancer. *Nature*, *486*(7404), 532–536. https://doi.org/10.1038/nature11156

Molinari, C., Marisi, G., Passardi, A., Matteucci, L., De Maio, G., & Ulivi, P. (2018). Heterogeneity in colorectal cancer: A challenge for personalized medicine? *International Journal of Molecular Sciences*, *19*(12). https://doi.org/10.3390/ijms19123733

Okada, Y., Kimura, T., Nakagawa, T., Okamoto, K., Fukuya, A., Goji, T., Fujimoto, S., Sogabe, M., Miyamoto, H., Muguruma, N., Tsuji, Y., Okahisa, T., & Takayama, T. (2017). EGFR downregulation after anti-EGFR therapy predicts the antitumor effect in colorectal cancer. *Molecular Cancer Research*, *15*(10), 1445–1454. https://doi.org/10.1158/1541-7786.MCR-16-0383

Perez-Riverol, Y., Csordas, A., Bai, J., Bernal-Llinares, M., Hewapathirana, S., Kundu, D. J., Inuganti, A., Griss, J., Mayer, G., Eisenacher, M., Pérez, E., Uszkoreit, J., Pfeuffer, J., Sachsenberg, T., Yilmaz, ., Tiwary, S., Cox, J., Audain, E., Walzer, M., … Vizcaíno, J. A. (2019). The PRIDE database and related tools and resources in 2019: Improving support for quantification data. *Nucleic Acids Research*, *47*(D1), D442–D450. https://doi.org/10.1093/nar/gky1106

Pfaffl, M. W. (2006). Relative quantification. In T. Dorak (Ed.), *Real-time PCR* (pp. 64–82). International University Line.

Reid, Y., Storts, D., Riss, T., & Minor, L. (2004). Authentication of Human Cell Lines by STR DNA Profiling Analysis. *Assay Guidance Manual*, *Md*, 1–18. http://www.ncbi.nlm.nih.gov/pubmed/23805434

Robert Koch-Institut (Hrsg.) und Gesellschaft der epidemiologischen Krebsregister in Deutschland e.V. (Hrsg.). (2021). *Krebs in Deutschland für 2017 / 2018* (13. Ausgab). Rober Koch-Institut (Hrsg). https://doi.org/10.25646/8353

Robin, T., Capes-Davis, A., & Bairoch, A. (2020). CLASTR: The Cellosaurus STR similarity search tool - A precious help for cell line authentication. *International Journal of Cancer*, *146*(5), 1299–1306. https://doi.org/10.1002/ijc.32639

Roessler, S., Lin, G., Forgues, M., Budhu, A., Hoover, S., Mark Simpson, R., Wu, X., He, P., Qin, L. X., Tang, Z. Y., Ye, Q. H., & Wang, X. W. (2015). Integrative genomic and transcriptomic characterization of matched primary and metastatic liver and colorectal carcinoma. *International Journal of Biological Sciences*, *11*(1), 88–98. https://doi.org/10.7150/ijbs.10583

Ruprecht, B., Zaal, E. A., Zecha, J., Wu, W., Berkers, C. R., Kuster, B., & Lemeer, S. (2017). Lapatinib resistance in breast cancer cells is accompanied by phosphorylation-mediated reprogramming of glycolysis. *Cancer Research*, *77*(8), 1842–1853. https://doi.org/10.1158/0008-5472.CAN-16-2976

Russo, M., Crisafulli, G., Sogari, A., Reilly, N. M., Arena, S., Lamba, S., Bartolini, A., Amodio, V., Magrì, A., Novara, L., Sarotto, I., Nagel, Z. D., Piett, C. G., Amatu, A., Sartore-bianchi, A., Siena, S., Bertotti, A., Trusolino, L., Corigliano, M., … Bardelli, A. (2019). Adaptive mutability of colorectal cancers in response to targeted therapies. *Science*, *366*(December), 1473–1480. https://doi.org/10.1126/science.aav4474

Sakamoto, A., Kato, K., Hasegawa, T., & Ikeda, S. (2018). An Agonistic Antibody to EPHA2 xhibits Antitumor Effects on Human Melanoma Cells. *Anticancer Research*, *38*, 3273–3282. https://doi.org/10.21873/anticanres.12592

Sayagués, J. M., Corchete, L. A., Gutiérrez, M. L., Sarasquete, M. E., Abad, M. del M., Bengoechea, O., Fermiñán, E., Anduaga, M. F., del Carmen, S., Iglesias, M.,

Esteban, C., Angoso, M., Alcazar, J. A., García, J., Orfao, A., & Muñoz-Bellvis, L. (2016). Genomic characterization of liver metastases from colorectal cancer patients. *Oncotarget*, *7*(45), 72908–72922. https://doi.org/10.18632/oncotarget.12140

Schneider, C. A., Rasband, W. S., & Eliceiri, K. W. (2012). NIH Image to ImageJ: 25 years of image analysis. *Nature Methods*, *9*(7), 671–675. https://doi.org/10.1038/nmeth.2089

Scott, P. H., Brunn, G. J., Kohn, A. D., Roth, R. A., & Lawrence, J. C. (1998). Evidence of insulin-stimulated phosphorylation and activation of the mammalian target of rapamycin mediated by a protein kinase B signaling pathway. *Proceedings of the National Academy of Sciences of the United States of America*, *95*(13), 7772–7777. https://doi.org/10.1073/pnas.95.13.7772

Song, N., Liu, S., Zhang, J., Liu, J., Xu, L., Liu, Y., & Qu, X. (2014). Cetuximab-induced MET activation acts as a novel resistance mechanism in colon cancer cells. *International Journal of Molecular Sciences*, *15*(4), 5838–5851. https://doi.org/10.3390/ijms15045838

Stehelin, D., Varmus, H. E., Bishop, J. M., & Vogt, P. K. (1976). DNA related to the transforming gene(s) of avian sarcoma viruses is present in normal avian DNA. *Nature*, *260*, 170–173. https://doi.org/10.1038/260170a0

Stintzing, S., Fischer von Weikersthal, L., Decker, T., Vehling-kaiser, U., Jäger, E., Heintges, T., Stoll, C., Giessen, C., Modest, D. P., Neumann, J., Jung, A., Kirchner, T., Scheithauer, W., & Heinemann, V. (2012). FOLFIRI plus cetuximab versus FOLFIRI plus bevacizumab as first-line treatment for patients with metastatic colorectal cancer-subgroup analysis of patients with KRAS: Mutated tumours in the randomised German AIO study KRK-0306. *Annals of Oncology*, *23*(7), 1693–1699. https://doi.org/10.1093/annonc/mdr571

Stintzing, S., Wirapati, P., Lenz, H. J., Neureiter, D., Fischer von Weikersthal, L., Decker, T., Kiani, A., Kaiser, F., Al-Batran, S., Heintges, T., Lerchenmüller, C., Kahl, C., Seipelt, G., Kullmann, F., Moehler, M., Scheithauer, W., Held, S., Modest, D. P., Jung, A., … Heinemann, V. (2019). Consensus molecular subgroups (CMS) of colorectal cancer (CRC) and first-line efficacy of FOLFIRI plus cetuximab or bevacizumab in the FIRE3 (AIO KRK-0306) trial. *Annals of Oncology : Official Journal of the European Society for Medical Oncology*, *30*(11), 1796–1803. https://doi.org/10.1093/annonc/mdz387

Szklarczyk, D., Morris, J. H., Cook, H., Kuhn, M., Wyder, S., Simonovic, M., Santos, A., Doncheva, N. T., Roth, A., Bork, P., Jensen, L. J., & von Mering, C. (2017). The STRING database in 2017: Quality-controlled protein-protein association networks, made broadly accessible. *Nucleic Acids Research*, *45*(D1), D362–D368. https://doi.org/10.1093/nar/gkw937

Thomas, C. C., Deak, M., Alessi, D. R., & Van Aalten, D. M. F. (2002). High-resolution structure of the pleckstrin homology domain of protein kinase B/Akt bound to phosphatidylinositol (3,4,5)-trisphosphate. *Current Biology*, *12*(14), 1256–1262. https://doi.org/10.1016/S0960-9822(02)00972-7

Tyanova, S., Temu, T., Sinitcyn, P., Carlson, A., Hein, M. Y., Geiger, T., Mann, M., & Cox, J. (2016). The Perseus computational platform for comprehensive analysis of (prote)omics data. *Nature Methods*, *13*(9), 731–740. https://doi.org/10.1038/nmeth.3901

Van Cutsem, E., Köhne, C. H., Hitre, E., Zaluski, J., Chien, C. R. C., Makhson, A., D'Haens, G., Pintér, T., Lim, R., Bodoky, G., Roh, J. K., Folprecht, G., Ruff, P., Stroh, C., Tejpar, S., Schlichting, M., Nippgen, J., & Rougier, P. (2009). Cetuximab and chemotherapy as initial treatment for metastatic colorectal

cancer. *New England Journal of Medicine*, *360*(14), 1408–1417. https://doi.org/10.1056/NEJMoa0805019

Van Cutsem, E., Köhne, C. H., Láng, I., Folprecht, G., Nowacki, M. P., Cascinu, S., Shchepotin, I., Maurel, J., Cunningham, D., Tejpar, S., Schlichting, M., Zubel, A., Celik, I., Rougier, P., & Ciardiello, F. (2011). Cetuximab plus irinotecan, fluorouracil, and leucovorin as first-line treatment for metastatic colorectal cancer: Updated analysis of overall survival according to tumor KRAS and BRAF mutation status. *Journal of Clinical Oncology*, *29*(15), 2011–2019. https://doi.org/10.1200/JCO.2010.33.5091

Van Cutsem, E., Lenz, H. J., Köhne, C. H., Heinemann, V., Tejpar, S., Melezínek, I., Beier, F., Stroh, C., Rougier, P., Han Van Krieken, J., & Ciardiello, F. (2015). Fluorouracil, leucovorin, and irinotecan plus cetuximab treatment and RAS mutations in colorectal cancer. *Journal of Clinical Oncology*, *33*(7), 692–700. https://doi.org/10.1200/JCO.2014.59.4812

Vincenzi, B., Zoccoli, A., Pantano, F., Venditti, O., & Galluzzo, S. (2010). CETUXIMAB: From Bench to Bedside. *Current Cancer Drug Targets*, *999*(999), 1–16. https://doi.org/10.2174/1568210200887900096

Weinberg, R. A. (2014). *The Biology of Cancer* (2nd editio). Garland Science, Taylor & Francis Group, LLC.

Woolston, A., Khan, K., Spain, G., Barber, L. J., Griffiths, B., Gonzalez-Exposito, R., Hornsteiner, L., Punta, M., Patil, Y., Newey, A., Mansukhani, S., Davies, M. N., Furness, A., Sclafani, F., Peckitt, C., Jiménez, M., Kouvelakis, K., Ranftl, R., Begum, R., … Gerlinger, M. (2019). Genomic and Transcriptomic Determinants of Therapy Resistance and Immune Landscape Evolution during Anti-EGFR Treatment in Colorectal Cancer. *Cancer Cell*, *36*(1), 35-50.e9. https://doi.org/10.1016/j.ccell.2019.05.013

Zhuang, G., Brantley-Sieders, D. M., Vaught, D., Yu, J., Xie, L., Wells, S., Jackson, D., Muraoka-Cook, R., Arteaga, C., & Chen, J. (2010). Elevation of receptor tyrosine kinase EphA2 mediates resistance to trastuzumab therapy. *Cancer Research*, *70*(1), 299–308. https://doi.org/10.1158/0008-5472.CAN-09-1845

7 ATTACHMENTS

7.1 ATTACHMENT 1: SUPPLEMENTARY MATERIALS AND METHODS

LC-MS/MS analyses were performed by Dr. Anna Jarzab at the Chair of Proteomics of the Technical University of Munich. The following materials and methods section has been kindly provided by Dr. Jarzab.

Cell lysis

For LC-MS/MS proteomic analysis cells were washed twice with ice-cold PBS and lysed in 500µl of 8M urea buffer in 80mM Tris-HCl, pH 7,6, supplemented with protease (Hoffmann-La Roche, Basel, Switzerland) and phosphatase inhibitors (Sigma Aldrich, St. Louis, MO, USA). Lysates were cleared by centrifugation at $10^5 \times g$ for 30 min at 4°C. Protein concentration was determined by Bradford assay (Coomasie Protein Assay Reagent, Thermo Fisher Scientific).

Proteolysis, TMT-labelling and peptide fractionation

Cell lysates were adjusted to 1mg/ml and 100µg proteins from each biological replicate were reduced with 10mM DTT for 45min at 37°C and alkylated with 55mM chloro-acetamide for 30min at room temperature in the darkness. Lysates were diluted with 5 volumes of 40mM Tris-HCl, pH 7,6 to decrease the concentration of urea prior trypsinisation. Proteolysis was performed by adding trypsin (Promega, Mannheim, Germany) in a 1:50 (w/w) enzyme-to-substrate ratio and incubating overnight at 37°C in a thermoshaker at 700rpm. On the next day samples were acidified by addition of formic acid (FA) to a concentration of 0,5% (v/v) to stop proteolysis and desalted using self-packed stage-tips (10 discs, Ø 1,5mm, C18 material, 3M EmporeTM Octadecyl C18, Saint Paul, MN, USA; wash solvent: 0,1% FA; elution solvent: 60% ACN in 0,1% FA). Peptide solutions were frozen at -80°C and dried in a SpeedVac. 100µg of protein hydrolysates were dissolved in 50mM HEPES, pH ,.5 for 10min at 20°C. TMT reagent (Thermo Fisher Scientific), dissolved in 100% anhydrous acetonitrile (can) was added to each vial to the final concentration of 11,6mM. Samples were incubated at 400rpm on a thermomixer for 1 hour at 20°C. The reaction was stopped by adding hydroxylamine to a final concentration of 0,4% and incubated for 15 min at 20°C at 400rpm. Labelled peptide solutions were pooled and desalted on 50mg Sep-Pak tC18, reversed-phase (RP) solid-phase extraction cartridges (Waters Corp., Finglas, Ireland; wash solvent: 0,1% FA; elution solvent: 60% CAN in 0,1% FA). TMT-labelled sample pools were fractionated on a Trinity P1 column (Thermo Fisher Scientific) using a Dionex Ultimate 3000 HPLC System (Dionex Corporation, Idstein, Germany) at a flow rate of 300µl/min. 100µg of protein hydrolysates were loaded onto the column in solvent A (10mM ammonium acetate in water, pH 4,7) and separated in a gradient of solvent B (95% acetonitrile in 10mM ammonium acetate, pH 5,4). Samples were collected in 32 fractions, dried down in a SpeedVac and measured on LC-MS.

LC-MS/MS analysis

1µg of each fraction was resuspended in 0,1% FA in water and injected into an Ultimate 3000 SD HPLC (Thermo Fisher Scientific) coupled to a Q Exactive HF (Thermo Fisher Scientific). Peptides were delivered to a trap column (75µm x 2cm,

packed in house with 5µm C18 resin, Reprosil PUR AQ, Dr. Maisch, Ammerbuch, Germany) for 10 min at a flow rate of 5µl/min in loading solvent (0,1% FA in water) and separated on the analytical column (75µm x 45cm, packed in house with 3µm C18 resin, Reprosil Gold, Dr. Maisch) using a 90 min gradient (solvent A: 0,1% FA, 5% DMSO; solvent B: 0,1% FA, 5% DMSO in ACN). The Q-Exactive HF was operated in data-dependent acquisition (DDA) and positive ion mode, automatically switching between MS1 and MS2. Full-scan MS1 spectra were acquired from 360 to 1300m/z, 60 000 resolution, automatic gain control (AGC) target value of 3 x 106 charges and a maximum injection time (maxIT) of 10ms. 25 precursor ions were permitted to be selected for fragmentation. MS2 spectra were acquired at 100 to 1200m/z at 30,000 resolution to enable resolution of all TMT labels, AGC target value of 1 x 103 charges and maximum injection time of 55ms.

Database searching and data analysis

Peptide and protein identification and quantification were performed using MaxQuant (v1.5.5.1) with embedded Andromeda search engine. Spectra were searched against the UniProt databases (human, 48 556 entries, downloaded on 19.07.2017). Trypsin/P was selected as proteolytic enzyme and up to two missed cleavage sites were allowed. Carbamido-methylation of cysteine was set up as fixed modifications and oxidation of methionine, and-N-terminal protein acetylation as variable modifications. The mass tolerance of precursor ions was set to 5ppm and for fragmentation to 20ppm. An FDR cut-off of 0,01 was used for identification of peptides and proteins. To facilitate further data analysis, the results were imported into the MaxQuant associated software suite Perseus (v.1.5.4.1). Quantification was performed TMT based. A Benjamini-Hochberg FDR corrected two-sided student's *t* test was used to assess statistical significance (FDR<0.05, S0 of 0.1).

Data accessibility

The mass-spectrometry proteomics data have been deposited to the ProteomeXchange Consortium via the PRIDE partner repository with the dataset identifier PXD022072 (Perez-Riverol et al., 2019).

AFFIDAVIT

I, Lucien Edward Torlot, hereby declare that the submitted thesis entitled

Proteomics uncover EPHA2 in cetuximab resistant colorectal cancer cell lines as a potential novel therapeutic target

is my own work. I have only used the sources indicated and have not made unauthorised use of services of a third party. Where the work of others has been quoted or reproduced, the source is always given.

I further declare that the dissertation presented here has not been submitted in the same or similar form to any other institution for the purpose of obtaining an academic degree.

Munich, 22.03.2023 Lucien Edward Torlot

PUBLICATIONS

Torlot, L., Jarzab, A., Kumbrink, J., Kirchner, T., Kuster, B., & Jung, A. (2018). Poster: (Phospho)proteomics uncover kinome reprogramming in cetuximab resistant colorectal cancer cell lines. *DKTK 5th Munich Cancer Retreat*.

Torlot, L., Jarzab, A., Albert, J. et al. Proteomics uncover EPHA2 as a potential novel therapeutic target in colorectal cancer cell lines with acquired cetuximab resistance. J Cancer Res Clin Oncol 149, 669–682 (2023). https://doi.org/10.1007/s00432-022-04416-0

ACKNOWLEDMENTS

I wish to express my sincere gratitude to Prof. Dr. Andreas Jung and to PD Dr. Jörg Kumbrink in helping me plan and finance my project, structure my work and answer my many questions.

My gratitude also goes out to

Agnes Pok-Udvari and Sabine Sagebiel-Kohler for the valuable lessons in lab work and their outstanding technical assistance throughout the project;

Dr. Anna Jarzab and Prof. Bernhard Kuster (Chair of Proteomics, TUM) for their help planning and performing the mass-spectrometric analysis;

Dr. Alberto Bardelli (Candiolo Cancer Institute, Italy) for providing the cell lines used in this study;

Prof. Dr. med. Volker Heinemann and Dr. Marco Gerlinger for kindly providing the clinical and transcriptomic data from the FIRE-3 and Prospect-C trials;

The unit of Molecular Pathology at the Institute of Pathology (LMU) – Gaby Charell, Ina Hochrein, Jutta Hügel-Tegge, Sabine Jung, Nicole, Perera, Konstanze Schäfer, Lisa Schneider, Darius Yazdanpanah – for their support with Next Generation Sequencing of samples;

Prof. Dr.med. Thomas Kirchner (Institute of Pathology, LMU) for his interest and support of the project.

I wish to thank Anna Patricia Schön and my parents for their unwavering moral support throughout the years I worked on this project.